CHALMERS
UNIVERSITY OF TECHNOLOGY

Preparation of auto-pilots for simple task execution and flight qualities assessment

A study on the design and use of controllers to substitute human pilots to asses aircraft flight qualities in simulation.

Master's thesis in Systems, Control and Mechatronics

ANDREAS ZETTERLUND
JORDAN HARVEY

DEPARTMENT OF ELECTRICAL ENGINEERING

CHALMERS UNIVERSITY OF TECHNOLOGY
Gothenburg, Sweden 2023
www.chalmers.se

Master's thesis 2023

Preparation of auto-pilots for simple task execution and flight qualities assessment

A study on the design and use of controllers to substitute human pilots to asses aircraft flight qualities in simulation.

Andreas Zetterlund
Jordan Harvey

CHALMERS
UNIVERSITY OF TECHNOLOGY

Department of Electrical Engineering
Division of Systems and Control
Chalmers University of Technology
Gothenburg, Sweden 2023

Preparation of auto-pilots for simple task execution and flight qualities assessment.
A study on the design and use of controllers to substitute human pilots to asses aircraft flight qualities in simulation.
Andreas Zetterlund, Jordan Harvey

Supervisor: Kenzo Sasaki, Heart Aerospace
Examiner: Jonas Fredriksson, Electrical Engineering

Master's Thesis 2023
Department of Electrical Engineering
Division of Systems and Control
Chalmers University of Technology
SE-412 96 Gothenburg
Telephone +46 31 772 1000

Cover: Render of the Heart Aerospace ES-30 commercial electric aircraft.

Typeset in LaTeX
Printed by Chalmers Reproservice
Gothenburg, Sweden 2023

Preparation of auto-pilots for simple task execution and flight qualities assessment
A study on the design and use of controllers to substitute human pilots in performing simple, repetitive tasks to asses aircraft flight qualities in simulation

Andreas Zetterlund
Jordan Harvey

Department of Electrical Engineering
Chalmers University of Technology

Abstract

In this project, an autopilot able to perform a defined set of manoeuvres has been developed and evaluated. The autopilot was developed to be used as a tool to gain insight into the flight qualities of an aircraft in simulation without the need for a test pilot. A baseline version was developed using cascaded PID controllers before a model-based approach was created using LQI controllers. A method of automatically testing all the operational conditions of the aircraft was developed together with a post-processing tool to quickly evaluate and warn the user of a non-satisfactory flight test. The autopilot proved able to take off, land and perform a rolling manoeuvre with and without one of four motors inoperable as well as in some cases handle wind disturbance. The model-based approach proved capable of handling changes in the aircraft model without the need to tune or adjust the controllers. The autopilot was able to provide repeatable and meaningful results over a large number of cases, however, did not fully remove the need for a test pilot.

Keywords: aircraft, autopilot, control theory, PID, LQI, linearization, simulation, trajectory tracking

Acknowledgements

We would like to thank our academic examiner and supervisor from Chalmers, Professor Jonas Fredriksson, for sharing his knowledge, enthusiasm and support throughout this thesis. Your support and positive attitude made the entire process enjoyable and left us free to grow and learn.

We must also give a special thanks to Kenzo Sasaki, our supervisor from Heart Aerospace. for taking the time to share his great knowledge of aerospace and flight mechanics. This thesis would not have been possible without you and your clear passion for the field was a great boost throughout.

Finally, to Andre Gama de Almeida, Ethem Hakan Orhan and the rest of the flight science department we must express our sincerest thanks for welcoming us as part of the team and enthusiastically sharing their many years of combined knowledge and experience. This was truly a great opportunity and made all the better by the people we met along the way.

Andreas Zetterlund
Jordan Harvey
Gothenburg, June 2023

List of Acronyms

Below is the list of acronyms that have been used throughout this thesis listed in alphabetical order:

AEO	all engines operable
AOA	angle of attack
COG	centre of gravity
DOF	degrees of freedom
EASA	European Union Aviation Safety Agency
EOM	equations of motion
LQI	linear quadratic integrator
OEI	one engine inoperable
PID	proportional-integral-derivative
TAS	true airspeed
VMO	maximum operating speed
VR	rotation speed
VSR	stall speed

Nomenclature

Below is the nomenclature of variables that have been used throughout this thesis.

Variables

α	Angle of attack
β	Sideslip angle
γ	Flight path angle
ϕ	Roll angle
θ	Pitch angle
ψ	Yaw angle
n_z	Vertical acceleration
H	Altitude
P	Roll Rate
Q	Pitch Rate
R	Yaw Rate
U	x velocity
Y	y velocity
Z	z velocity
n_z	Vertical Acceleration
H	Altitude

Contents

List of Figures

List of Tables

1
Introduction

Aircraft have existed since the 1900s and have since undergone continuous improvement with longer ranges, bigger passenger capacity, and more sustainable fuels being introduced. In 2019 Heart Aerospace announced that they were producing the first electric aircraft for the commercial market. Developing a new aircraft requires a great amount of work to be done in simulation, including certification tests and flight quality assessment. As part of the certification process, the aircraft has to prove it is capable of completing a range of tests and manoeuvres. During the development phase, these manoeuvres are commonly performed by an experienced test pilot that will fly the aircraft in a controlled and simulated environment using hardware-in-loop simulators. These manoeuvres are performed continuously throughout the development phase to ensure that changes made to the aircraft have not altered its flight qualities in a negative manner. Later in the certification phase, the same manoeuvres will have to be performed in the air with the actual aircraft.

This thesis focuses on automating the process of performing the required manoeuvres in simulation. This automated process is developed to speed up the design phase in the aviation industry and allow for faster iterations to get faster feedback on the design choices without requiring a test pilot in order to run through all test cases.

1.1 Background

For many years the aerospace industry has been dominated by a few large companies such as Airbus and Boeing [1]. These large companies continuously develop new generations of aircraft with higher efficiency and better capacity however, for the last 70 years they have all been modifications to existing aircraft with no large innovations [2]. This demonstrates how the commercial aerospace industry is currently moving at a very slow pace as it is no longer cost-efficient to create completely new models. One of the reasons for the slow development time for an aircraft is the large amounts of regulations and requirements from governing bodies such as the European Union Aviation Safety Agency (EASA) [3]. These regulations are in place to ensure the safety and handling qualities of the aircraft. The CS-25 standard includes several manoeuvres that have to be carried out by the aircraft in order to prove that the aircraft meets the requirements. These tests can include manoeuvres such as stalling, high banking angle turns, and landing with engine failure, all of which are done by a test pilot.

Aircraft are highly complex systems with many different types of systems being developed simultaneously making them very susceptible to an iterative design process, see e.g., [4] and [5]. Any change to one system is likely to have an effect on another. In an effort to optimise performance and meet regulatory requirements, these systems are prone to many changes and alterations throughout the design process. This in turn requires tests and analysis to be performed multiple times as the aircraft continues to evolve to ensure that all requirements are met and that improvements in one area have not had significant adverse effects in other areas.

1.1.1 Autopilot

The first autopilot was developed in 1912 by the Sperry Corporation and enabled an aircraft to fly on a fixed compass bearing and fixed altitude with no pilot inputs [6]. In 1931 a commercial plane had an autopilot installed for the first time in history and over the past century, autopilots have become more and more standard, with international aviation regulations making them mandatory in some categories of aircraft. The earlier Sperry-based autopilots were used as pilot relief modes and could hold a desired attitude and speed. Typically these autopilots would hold the aircraft within certain bounds with limited control authority and notify the pilot if the bounds or control limits were reached [7]. Over the course of the last nine decades, autopilots have advanced greatly with current technology offering many features including automated takeoff, go-around, and trimming as well as nav-to-nav captures, vertical intercepts, and many procedure manoeuvres [8].

In recent years, research has been focusing on increased handling of adverse flight conditions or increased auto-landing capabilities [9][10][11]. Generally, the autopilots designed in literature are designed for a specific purpose, commonly either heading and altitude tracking while in the air or the performance of a specific manoeuvre such as takeoff or landing. Although able to better handle complex situations or tricky flight conditions these controllers are more challenging to design and implement and require a more accurate model. Another research direction that is gaining momentum is in the design of autopilots for UAVs and autonomous aircraft, see [12] and [13]. Recent technological advancements have allowed UAVs to rapidly grow in popularity, motivating research in the field. Taking inspiration from research on conventional aircraft autopilots the field has advanced rapidly however many commercial autopilot systems still depend on PID controllers [14].

The field of research investigating pilot models is a complex and multidisciplinary area including both mathematical representations and human factors [15]. Motivated by increased challenges stemming from aerospace advances such as flexible airframes and fly-by-wire control, research in this field has been largely influential in the definition of handling qualities for aircraft. There is however a lack of examples where a pilot model is used to hasten the development process of new aircraft. The multiple iterations and ever-evolving design typical in the aerospace industry could benefit from having an autopilot able to perform a set of standard manoeuvres

and feedback in a way not dissimilar to test-driven development commonly used in software development [16].

Going forward it is important to note what is meant by the use of the term autopilot in the context of this project. Although modern autopilots are extremely advanced, with some able to perform or assist in takeoffs and landings, it is common for discussions about autopilots to centre around functions such as altitude hold, envelope protection, or other similar pilot relief functions [17]. In the context of this project the term *autopilot* is used to refer to a controller that is able to act independently of human input and perform manoeuvres automatically. Where autopilots in aircraft are used to help pilots, the one developed here is used to replace the pilot in simulation.

1.1.2 The aircraft

The aircraft used as a reference for this thesis is a reserve hybrid aircraft being run on 4 electric motors with one propeller per motor, the aircraft is also known as Heart Aerospace ES-30. It uses a battery as its primary energy source, with a turbo-generator to extend its range from 200km using only battery power, to 400km using the turbo generator. The aircraft carries up to 30 passengers based on the configuration. With electric propulsion, the aircraft is designed to be able to run on zero emissions when using only the battery on flights under 200km.

1.1.3 Flight qualities

An aircraft's flying quality can be determined in many possible ways and using different scales. A common way to look at the flight qualities of an aircraft from a pilot's perspective is to use the Cooper-Harper scale commonly used in the aerospace industry, [18]. This is a scale based on a point system from 1-10 where 1 indicates the best and 10 the worst. The test pilots perform a certain manoeuvre and rank the aircraft's handling qualities using a set of criteria. In this thesis, the flight qualities are based on the stability of the aircraft, disturbance handling, and its capability of performing the required manoeuvres rather than from a pilot's perspective.

1.2 Objective

The objective of this thesis is to investigate the possibility of evaluating flight qualities of an aircraft using an autopilot instead of a test pilot. These handling qualities that are tested are determined by the CS-25 standards. These standards are set as a minimum requirement as they form a part of the certification process. The autopilot should be able to perform the manoeuvre within the aircraft's centre of gravity (COG) envelope and provide an indication of whether or not the aircraft has passed the test.

The autopilot should be able to handle a changing model such that the need to

adjust or change the controller when the model changes is kept to an absolute minimum. The autopilot should additionally be able to handle the failure cases or disturbances described in the CS-25 standards.

1.3 Limitations

Due to the complexity of modelling, an in-house aircraft model is used as a basis for this project. The model is nonlinear with 6 degrees of freedom (DOF) and is used for controller design and testing. It assumes that all the states of the aircraft can be measured and that all sensors are perfect in the sense of no noise or latency in the measurements. Any disturbances experienced will be through wind as these cases are specifically requested in the CS-25 test cases. It is also assumed that there is a single command controlling all motors, meaning that thrust vectoring is not possible.

The CS-25 includes over 50 different test cases which test several types of scenarios including takeoff, landing, lateral and longitudinal manoeuvres. The scope of the project did not include every single test case but a minimum of one test case from each category was selected to validate the use of the autopilot. By using test cases from all categories it could be ensured that the autopilot was able to handle all types of manoeuvres and failures.

1.4 Ethics

Heart Aerospace aims to develop the ES-30, a reserve hybrid electric regional aircraft, which is able to transport people across impossible terrain quickly and in an environmentally friendly manner. This mode of transportation reduces the travel time, cost and also makes it more accessible compared to current solutions. One example of this is the Norwegian fjords where the only way to get between villages is either by slow ferries or by driving a car up and down mountain passes. This distance can more easily be covered by an electric aircraft in a short amount of time for a low cost. By switching the propulsion from a conventional turboprop engine to an electric motor there could be an estimated cost reduction of 50% in the long term [19]. The noise pollution around airports would be reduced drastically, increasing the possibility of building houses and living spaces closer to airports.

Electrifying the aerospace industry does have some negative consequences, however. The mining and production of the materials needed to produce batteries for electric vehicles is in itself harmful to the environment and often has negative impacts on the local communities [20]. Disposing of electronic waste is additionally quite challenging and as the electric aviation industry grows measures will need to be put in place to ensure the electronic waste is dealt with in an environmentally friendly manner [21]. The move to electric aircraft could also result in the loss of work as the skills required to produce electric aircraft are different from those required for traditional aircraft. While the transition to an electric aerospace industry has the potential to bring about many positive changes it does have the potential

to bring about harm as well.

In addition to the environmental aspects, there are also ethical challenges with the creation of an autopilot. The autopilot is attempting to simulate a human, however, every person is different and approaches things in different ways, therefore modelling a pilot is, in a sense, impossible. In aerospace, tests, and manoeuvres are performed with a real pilot in a simulation environment to gather data and gain an understanding of how the aircraft will perform. Making an autopilot that acts as the pilot could increase the amount of testing that can be performed and increase efficiency however, it could also remove the need for a real test pilot and potentially indicate a level of controllability impossible to achieve by a human. This could in turn cause the changes to the aircraft to go through design and production with potential problems unnoticed, and the consequences could be that the real aircraft is not safe to fly. There is additionally no way to guarantee that the autopilot, intended for simulation, is not used in the actual aircraft. Since it would not be designed for this there is a chance that it performs unexpectedly which could result in significant harm and damage. Finally, there is the question of whether this method of testing the aircraft's performance should be regarded as realistic enough considering these are the manoeuvres required to be able to certify the aircraft.

2
Model

The aircraft model used in this project was created and provided by Heart Aerospace. The model represented an early version of the ES-30 and, although not a perfect representation of the real world or final version of the ES-30, was considered to have the true dynamics for the purpose of this project. All controllers were designed for and validated using this model.

The modelling of aircraft have been extensively covered in literature and the derivation of the equations of motion (EOM) will not be covered here but can instead be found in [22] and [7]. Rather an overview of the model used in this project and a summary of any relevant material is provided in the following subsections.

2.1 Non-linear model

The EOM for an aircraft can be obtained from Newton's laws of motion:

$$\begin{aligned} m(\dot{U} + QW - RV) &= F_{G_x} + F_{A_x} + F_{T_x} \\ m(\dot{V} + RU - PW) &= F_{G_y} + F_{A_y} + F_{T_y} \\ m(\dot{W} + PV - QU) &= F_{G_z} + F_{A_z} + F_{T_z} \\ \dot{P}I_{xx} + QR(I_{zz} - I_{yy}) - (\dot{R} + PQ)I_{xz} &= M_{A_x} + M_{T_x} \\ \dot{Q}I_{yy} + PR(I_{zz} - I_{xx}) - (P^2 - R^2)I_{xz} &= M_{A_y} + M_{T_y} \\ \dot{R}I_{zz} + PQ(I_{yy} - I_{xx}) - (QR - \dot{p})I_{xz} &= M_{A_z} + M_{T_z} \end{aligned} \tag{2.1}$$

The first 3 equations represent the acceleration of the aircraft as a result of applied forces. The applied forces are grouped into 3 different components, F_G, F_A and F_T which correspond to gravitational, aerodynamic and thrust forces respectively. The last 3 equations are the moment equations with the moments coming from the aerodynamics (M_A) and thrust (M_T). These equations relate the applied moments to the resulting angular acceleration. The equations are expressed in the non-inertial, body frame. It should be noted that to fully solve the aircraft problem additional equations are required due to the presence of Euler angles in the force equations. These are not covered here but are discussed in detail in [22].

As previously mentioned, a complete aircraft model was provided as a basis for the thesis. The aircraft model was split up into 8 different Simulink models as seen in figure 2.1. The aerodynamics, ground and propulsion blocks model the forces

and moments caused by these effects. The control surfaces block took input commands from the pilot block and modelled the dynamics of the control surfaces being commanded. The weather block modelled wind, ice and rain which fed into the aerodynamics, propulsion and ground blocks as required. Finally, the equations of motion block took the forces and moments generated by the other blocks and combined them, modelling the effect of these forces and moments on a body with 6 degrees of freedom. All work performed in this thesis was done inside the pilot block. This enables the same model to be used for pilot tests with only the pilot block requiring alterations.

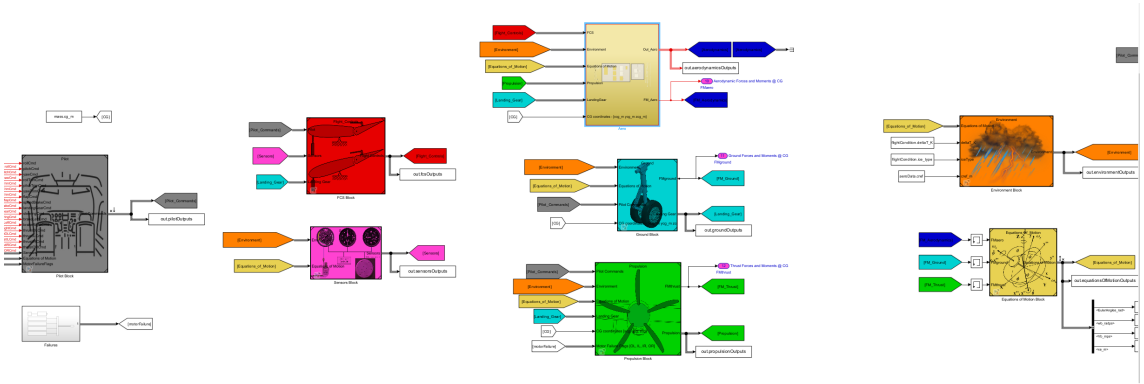

Figure 2.1: The aircraft model representing the ES-30 in Simulink.

The set of inputs to the model and the corresponding effect is shown in table 2.1. All commands are normalised and represent a certain deflection in degrees on the control surfaces or percentage thrust command.

Input	Range	Relevant control surface	Primary effect
Roll Command	−1 to 1	Ailerons	Rolling moment
Pitch Command	−1 to 1	Elevators	Pitching moment
Yaw Command	−1 to 1	Rudder	Yawing moment
Thrust Command	0 to 1	Motors	Thrust force

Table 2.1: Input control limits, control surface and primary effect.

The measured outputs from the model are assumed to be ideal with no measurement noise, delay or other disturbance. All variables are expressed in one of two reference frames, namely the body frame denoted by the subscript $_b$ and the inertial, or Earth, frame denoted by the subscript $_e$. The body axis is defined in relation to the aircraft with the origin placed at the COG, the x-axis pointing out the nose, the y-axis pointing out the right wing and the z-axis pointing down out the bottom of the aircraft following the right-hand rule convention as shown in figure 2.2. The earth axis is fixed to the Earth with the origin on the surface, z-axis pointing out the Earth and the x and y-axis lying in the local horizontal plane. The Euler angles representing roll, pitch and yaw describe the successive angles required to rotate the

body frame into the inertial frame. The yaw angle is defined as the angle between a projection of the body x-axis onto the earth xy-plane and the earth x-axis. The pitch angle is defined as the angle measured in a vertical plane between the body x-axis and the earth xy-plane. Finally, the roll angle is defined as the angle measured in the body yz-plane between the body y-axis and the Earth xy-plane [22]. A list of the most relevant outputs is given in table 2.2.

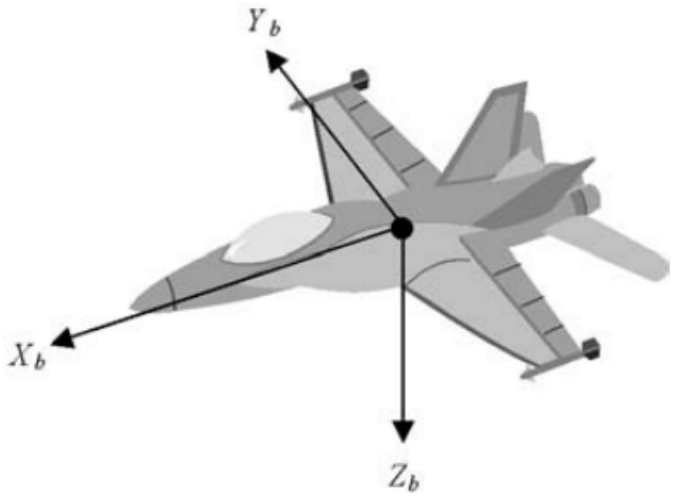

Figure 2.2: Aircraft body axis system [22].

Variable	Symbol	Units
Roll	ϕ	$degrees$
Pitch	θ	$degrees$
Yaw	ψ	$degrees$
Roll Rate	P	$degrees/s$
Pitch Rate	Q	$degrees/s$
Yaw Rate	R	$degrees/s$
Velocity in x-direction	U	m/s
Velocity in y-direction	V	m/s
Velocity in z-direction	W	m/s
True airspeed	TAS	m/s
Altitude	H	m
Acceleration in body z-axis	n_z	$g's$
angle of attack (AOA)	α	$degrees$
Side slip angle	β	$degrees$
Flight path angle	γ	$degrees$

Table 2.2: Table of output variables, symbols and units for aircraft model.

The angle of attack AOA refers to the angle between the chord line and velocity vector of the airflow approaching the wings, where the cord line is a straight line from the leading edge to the trailing edge of the wings. This is best illustrated in figure 2.3 below. The side slip angle is essentially the angle between the body xz-plane and the velocity vector of the perceived wind.

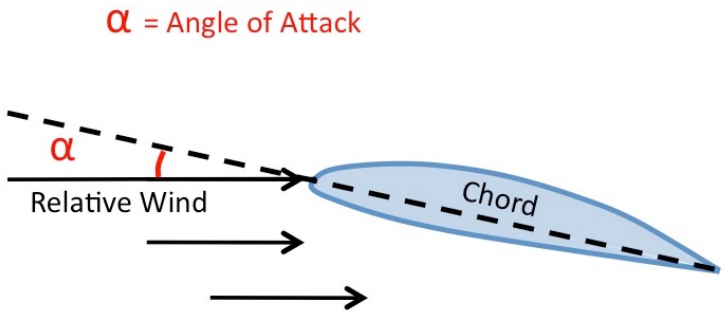

Figure 2.3: Angle of attack [23]

2.2 Trimming

For an aircraft to be steady in flight it has to be trimmed for the specific state and environmental conditions it is experiencing. This trimmed condition could be a steady climb, constant turn, level flight and so on. Pilots do this by adjusting

the throttle and control surfaces of the aircraft until the aircraft is stable in the desired state which relieves forces on the controls. For example, by adjusting the trim position of the horizontal stabiliser and throttle the aircraft can be made to fly at a constant pitch angle and airspeed without any inputs. This trimming needed to be done before any simulation or linearization of the model could be performed. The trimming was done on the nonlinear model through the MATLAB command `findop` which uses a gradient descent optimiser to find the local minimum where all accelerations are zero, or close to zero, ensuring a steady-state flight.

2.2.1 Gradient descent

Gradient descent is a method that uses iterative search to find a local minimum by taking small steps η in the direction of the negative derivative. The rate η determines how big of a step size the method takes for each iteration. Choosing η too high, can cause the method to not converge to a solution, due to overshooting the solution in each iteration, whilst picking a to short step size will make it unnecessarily slow to find the optimal solution [24].

Once this local minimum is found this becomes the initial conditions of the aircraft and is used as the baseline for all further simulations. If the aircraft is simulated in another state such as takeoff, landing, or at a different altitude then the aircraft needs to be re-trimmed with these conditions. If for example the aircraft is trimmed for takeoff where the flaps are in the downward position the aircraft has a completely different lift curve when compared to with flaps up which means that the aircraft trim solution would no longer hold true.

2.3 Linearization

Due to the model being nonlinear and many control and analysis methods requiring a linear plant, the model needed to be linearized. This linearization was done by choosing an operating point and calculating a linear approximation around that point. This operating point for the linearization was chosen as the trim point of the aircraft as this was both a stable point and the point around which the aircraft would be controlled. Any deviation that takes the aircraft away from the operating point would result in the linear system becoming less representative of the nonlinear system and cause the linear plant to be inaccurate. Matlab has a built-in command to find the linear model by specifying the nonlinear model and the operating point, `linearize(model,op)`. This function has multiple options however the method used involved a block-by-block linearization where each block in the model was individually linearized and the results combined [25].

The linearization process resulted in a state space model of the form:

$$\begin{aligned} \dot{x}(t) &= Ax(t) + Bu(t) \\ y(t) &= Cx(t) + Du(t) \end{aligned} \tag{2.2}$$

where $x(t)$ is the state vector, $u(t)$ is the input vector, and $y(t)$ is the output vector. A represents the state matrix representing the system dynamics, B represents the input matrix, C represents the output matrix, and D represents the feedthrough matrix.

The linearized model had 12 states, 16 inputs and 49 outputs. Many of the inputs and outputs could be neglected as they are not relevant to the controller design. This simplified the model to one with 4 inputs, described in table 2.1, and 15 outputs, described in table 2.2. The states consisted of those expected from the set of standard aircraft EOM which indicated a correct linearization with no additional dynamics, such as ground forces, being captured. Due to a combination of the non-linear model and the linearization process, many values in the state space were extremely small, typically of the order 10^{-8} or smaller. These terms were negated by simply approximating them to be equal to 0. It could then be noted that for this aircraft when trimmed in wings-level flight, the lateral and longitudinal dynamics were independent of each other. The lateral and longitudinal dynamics could then be separated and controllers independently designed for the separated dynamics [22]. The set of lateral and longitudinal states are described in table 2.3 below. This set of states and the ability to decouple the dynamics was constant for all trim points with wings level, although the actual values within the A and B state space matrices changed. Similarly, the structure of the A and B matrices was constant however the C and D matrices were subject to change depending on which outputs were selected. A possible example of the decoupled state space dynamics in the longitudinal and lateral direction is shown in equation 2.3 and 2.4 below.

Lateral States	Longitudinal States
ϕ	θ
ψ	Q
P	U_b
R	W_b
V_b	Z_e

Table 2.3: Table of lateral and longitudinal state variables used in decoupled model

$$\begin{bmatrix} \dot{\phi} \\ \dot{\psi} \\ \dot{p} \\ \dot{r} \\ \dot{\text{vb}} \end{bmatrix} = \underbrace{\begin{bmatrix} 0 & 0 & 1.0 & 0.1 & 0 \\ 0 & 0 & 0 & 1.0 & 0 \\ 0.0001 & 0 & -0.1 & 0.1 & -0.05 \\ -0.0001 & 0 & 0.01 & -0.1 & 0.01 \\ 10 & 0 & 5 & -50 & -0.1 \end{bmatrix}}_{A_{Lat}} \begin{bmatrix} \phi \\ \psi \\ p \\ r \\ \text{vb} \end{bmatrix} + \underbrace{\begin{bmatrix} 0 & 0 \\ 0 & 0 \\ 1 & -0.1 \\ -0.01 & 0.1 \\ 0 & -1 \end{bmatrix}}_{B_{Lat}} \begin{bmatrix} \text{rollCmd} \\ \text{yawCmd} \end{bmatrix}$$

$$\begin{bmatrix} \phi_{\text{deg}} \\ \psi_{\text{deg}} \end{bmatrix} = \underbrace{\begin{bmatrix} 57.2958 & 0 & 0 & 0 & 0 \\ 0 & 57.2958 & 0 & 0 & 0 \end{bmatrix}}_{C_{Lat}} \begin{bmatrix} \phi \\ \psi \\ p \\ r \\ \text{vb} \end{bmatrix} + \underbrace{\begin{bmatrix} 0 & 0 \\ 0 & 0 \end{bmatrix}}_{D_{Lat}} \begin{bmatrix} \text{rollCmd} \\ \text{yawCmd} \end{bmatrix} \quad (2.3)$$

$$\begin{bmatrix} \dot{\theta} \\ \dot{q} \\ \dot{\text{ub}} \\ \dot{\text{wb}} \\ \dot{\text{ze}} \end{bmatrix} = \underbrace{\begin{bmatrix} 0 & 1.0 & 0 & 0 & 0 \\ 0 & -1.0 & 0.01 & -0.01 & 0 \\ -10 & -5.0 & -0.01 & 0.1 & 0 \\ -5.0 & 50.0 & -0.1 & -1.0 & -0.001 \\ -50.0 & 0 & -0.1 & 1.0 & 0 \end{bmatrix}}_{A_{Long}} \begin{bmatrix} \theta \\ q \\ \text{ub} \\ \text{wb} \\ \text{ze} \end{bmatrix} + \underbrace{\begin{bmatrix} 0 & 0 \\ 1.0 & -0.01 \\ -0.1 & 1.0 \\ 1.0 & 0 \\ 0 & 0 \end{bmatrix}}_{B_{Long}} \begin{bmatrix} \text{pitchCmd} \\ \text{thrustOLCmd} \end{bmatrix}$$

$$\begin{bmatrix} \theta_{\text{deg}} \\ H_m \\ \text{TAS}_{\text{mps}} \\ \text{We}_{\text{mps}} \end{bmatrix} = \underbrace{\begin{bmatrix} 57.2958 & 0 & 0 & 0 & 0 \\ 0 & 0 & 0 & 0 & -1.0 \\ 0 & 0 & 0.9951 & 0.0986 & 0 \\ -50.0 & 0 & -0.1 & 1.0 & 0 \end{bmatrix}}_{C_{Long}} \begin{bmatrix} \theta \\ q \\ \text{ub} \\ \text{wb} \\ \text{ze} \end{bmatrix} + \underbrace{\begin{bmatrix} 0 & 0 \\ 0 & 0 \\ 0 & 0 \\ 0 & 0 \end{bmatrix}}_{D_{Long}} \begin{bmatrix} \text{pitchCmd} \\ \text{thrustOLCmd} \end{bmatrix} \tag{2.4}$$

Knowing the linearization would need to be repeated each time the aircraft was trimmed, this entire process was packaged into a single executable MATLAB script. Doing so made it possible to obtain the decoupled linearised models quickly and easily at any point and allowed other scripts or processes to get access to a linearised model of the correct flight configuration without the need to manually setup and run the linearization commands and decouple the dynamics by hand.

2.4 Linear system analysis

With the model in a linear form, analysis could be performed to gain insight into the system dynamics. It should be noted that as the obtained linearised model was dependent on factors such as the location of COG, flap configuration and attitude, the following analyses are for only one such case. For all analyses, the linear model refers to the exact output of the linearization process, before any simplifications, or decoupling was performed.

2.4.1 System validation

In order to see how well the linearised system captures the dynamics of the non-linear system around the operating point, the linear and non-linear models were fed the same input single and the correlating outputs were compared. A 0.5s square pulse with an amplitude of 0.1 was separately applied to the roll, pitch, yaw and thrust commands and the respective outputs were plotted. The most relevant for each are shown below with additional figures shown in appendix A.

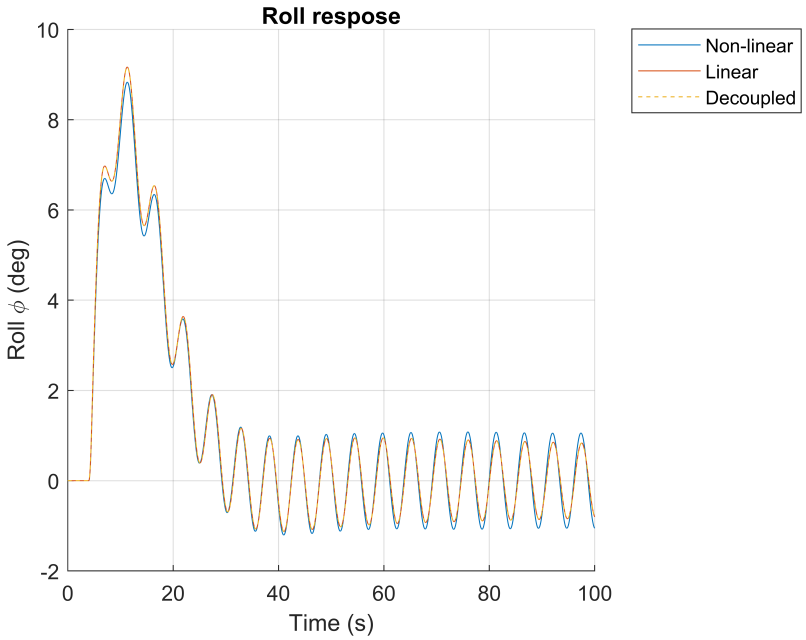

Figure 2.4: Roll response to a 0.5s square pulse with an amplitude of 0.1 applied to roll command

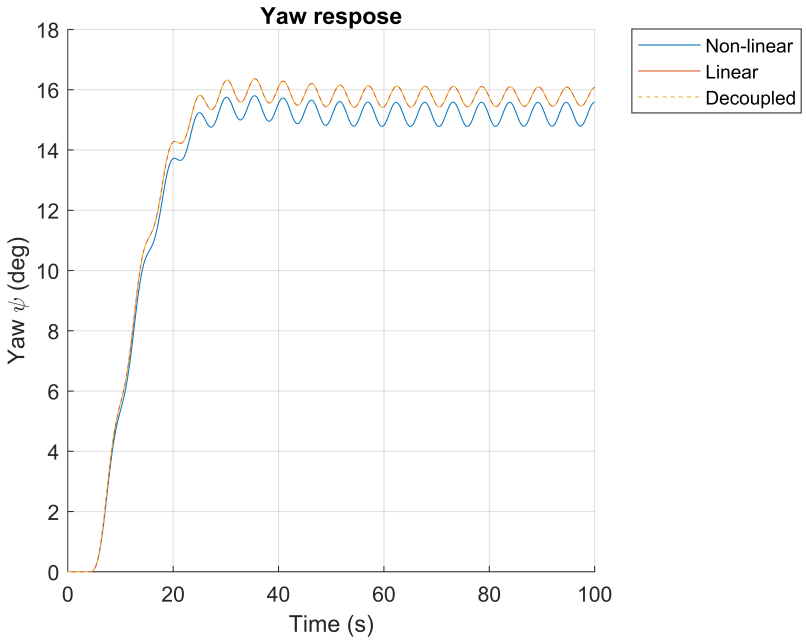

Figure 2.5: Yaw response to a 0.5s square pulse with an amplitude of 0.1 applied to roll command

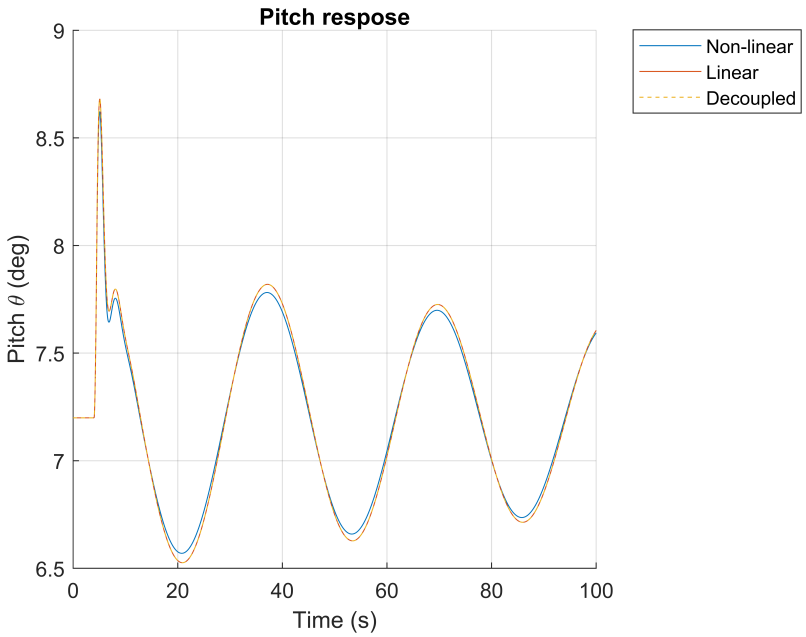

Figure 2.6: Pitch response to a 0.5s square pulse with an amplitude of 0.1 applied to pitch command

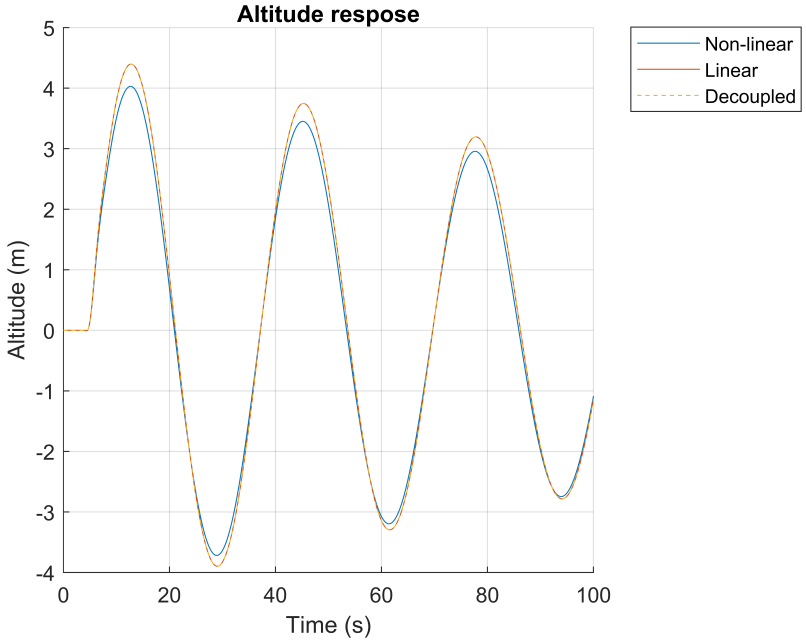

Figure 2.7: Altitude response to a 0.5s square pulse with an amplitude of 0.1 applied to pitch command

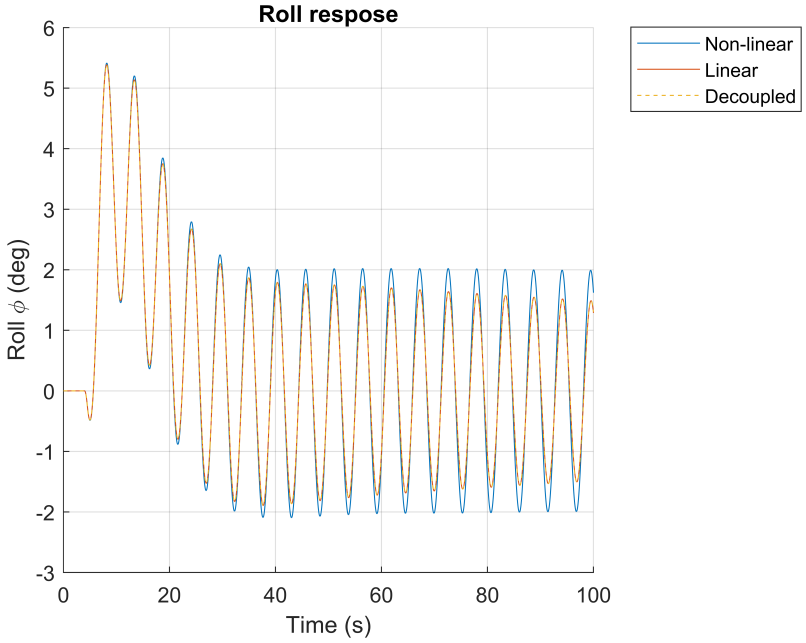

Figure 2.8: Roll response to a 0.5s square pulse with an amplitude of 0.1 applied to yaw command

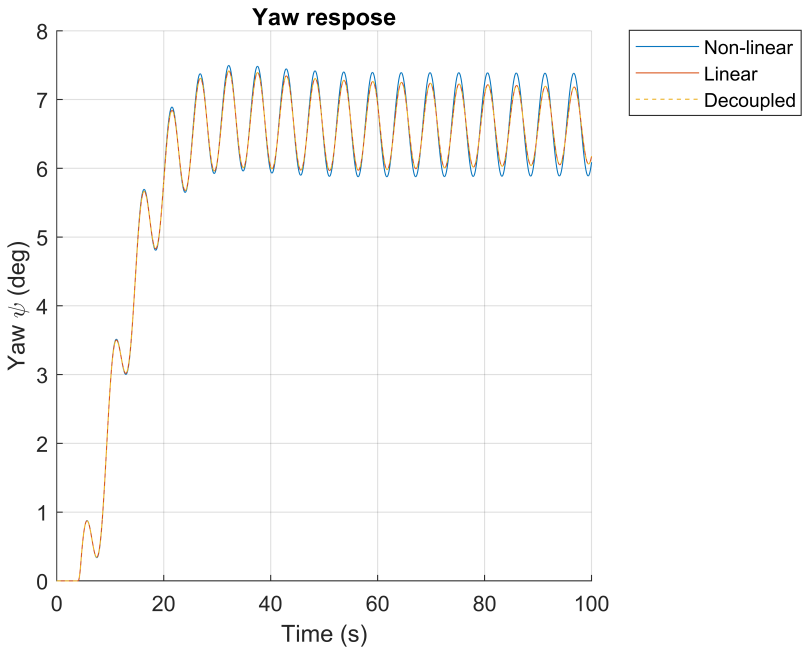

Figure 2.9: Yaw response to a 0.5s square pulse with an amplitude of 0.1 applied to yaw command

It could be noted that in all cases the linear and decoupled-linear systems performed almost identically. This indicated that the removal of the small terms in the state space model did not affect the dynamics in a significant way. It could also be noted that, when compared to the non-linear response, the linearized models were a very close match. The frequency of the dynamics matched perfectly with only small differences in amplitude when further from the operating point.

2.5 Flight mechanics

All aircraft have a number of modes that are characterised by their dynamic behaviour. The five modes present in aircraft can be separated into longitudinal and lateral-directional modes and their typical pole type and type of response are shown in table 2.4. These modes could be investigated by observing the location of the poles and zeros of the system.

Mode	Root type	Response
Longitudinal		
Short period	Complex conjugate	Oscillatory
Phugoid	Complex conjugate	Oscillatory
Lateral-directional		
Dutch roll	Complex conjugate	Oscillatory
Roll	Real	Nonoscillatory
Spiral	Real	Nonoscillatory

Table 2.4: Modes of Aircraft Motion, from [22].

The phugoid mode is present in longitudinal motion and is characterised by low-frequency and under-damped oscillations. It is a mode where energy is oscillating back and forth between potential energy and kinetic energy. The aircraft pitches up and thereby gains altitude and loses speed. As the aircraft slows down, the aerodynamic moment pitching the nose up lessens and the aircraft begins to pitch down, gaining speed and losing altitude. Once the aircraft has gained enough speed it begins to pitch up again and the cycle repeats. The phugoid mode can be unstable but due to the very slow period, sometimes up to 2 minutes with a minimal amplitude, it does not affect the aircraft in performing any precise manoeuvres and can easily be counteracted by a very small effort from the pilot. The poles responsible for this mode are typically complex with a low damping ratio and long time constant.

The short-period mode appears as a heavily damped oscillation in the longitudinal axis and is typically initiated by an impulse in the elevator command or a disturbance in the form of a wind gust in the vertical direction. This mode generally returns to trim within 1-5 seconds with an exponential or oscillatory trajectory. The poles for this mode are typically complex with a high damping ratio and short time constant. It is required by the CS25 certification that this mode is stable [3].

During motion, the aircraft will have an offset between the aircraft's direction of travel and the direction of the perceived wind which will result in some amount of side-slip β. This side-slip will cause a moment in roll and yaw which results in a coupled oscillation in both roll and yaw referred to as dutch roll. The dutch roll poles are typically complex with a low damping ratio or are unstable.

The roll mode is a simple mode with a typically stable, non-oscillatory response. When the aircraft rolls it increases the lift on the downwards-moving wing which naturally damps the motion caused by any impulse or disturbance about this axis. The time constant of this mode varies and largely depends on the desired level of manoeuvrability of the aircraft.

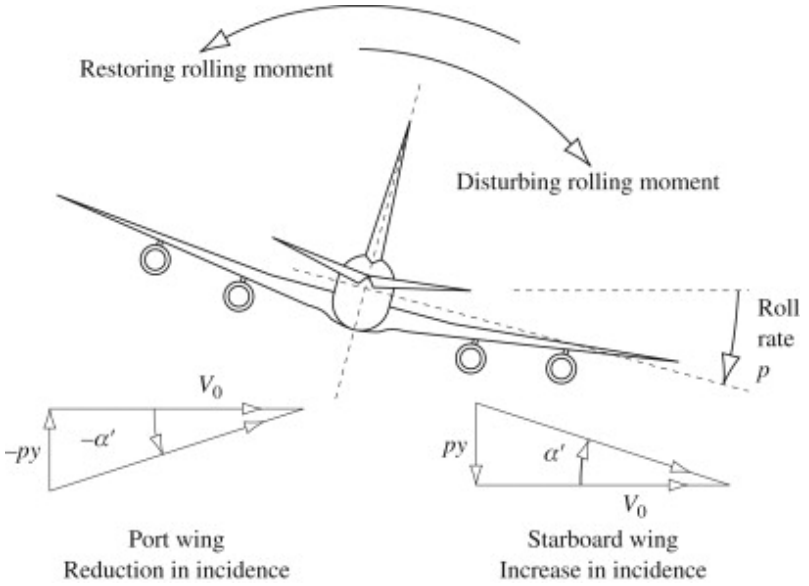

Figure 2.10: Restoring rolling moment in response to disturbance [26]

The spiral mode is a slow and often unstable mode that appears after a disturbance in the side-slip which is followed by a rolling moment. This rolling moment causes the aircraft to start spiralling and diverges in both roll and yaw. Since the aircraft is not in its trimmed condition and the vertical forces are not in equilibrium the aircraft starts to lose altitude as it spirals. This will cause the aircraft to eventually hit the ground if the spiral mode is left unchecked. The spiral mode usually has a large time constant of 100s or more [26].

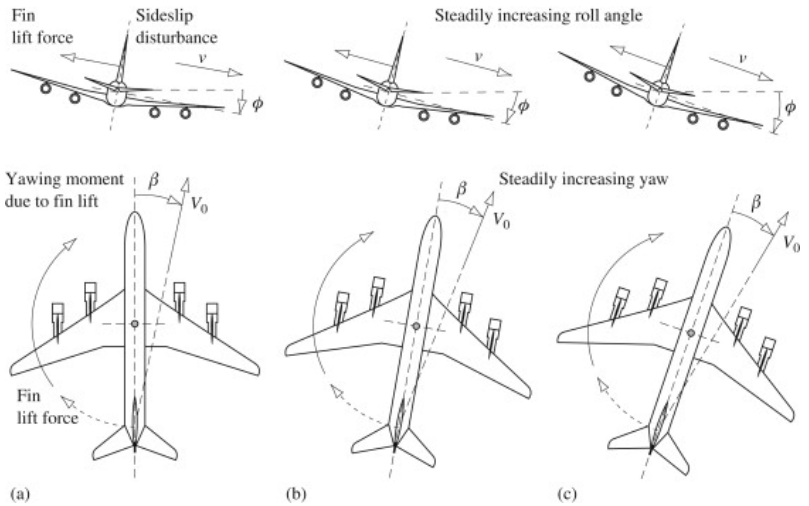

Figure 2.11: Illustration of the spiral mode [26]

By analysing the location of the poles of the linearized system, information can be gained regarding the aircraft's handling and its dynamic modes. The short period and phugoidal modes, described above, are a result of the poles from the longitudinal dynamics. The short period mode is a result of the poles furthest from the origin and the phugoidal mode results from the complex poles near the origin seen in figure

2.12. The position of the short-period poles indicated the mode would have a stable, oscillatory response with a fast response time while the phugoidal mode would also have a stable oscillatory response that is much slower. The effects of these poles can be clearly seen in figure 2.6 with the short period mode causing the quick spike at the beginning and the lightly damped oscillations being caused by the phugoidal mode.

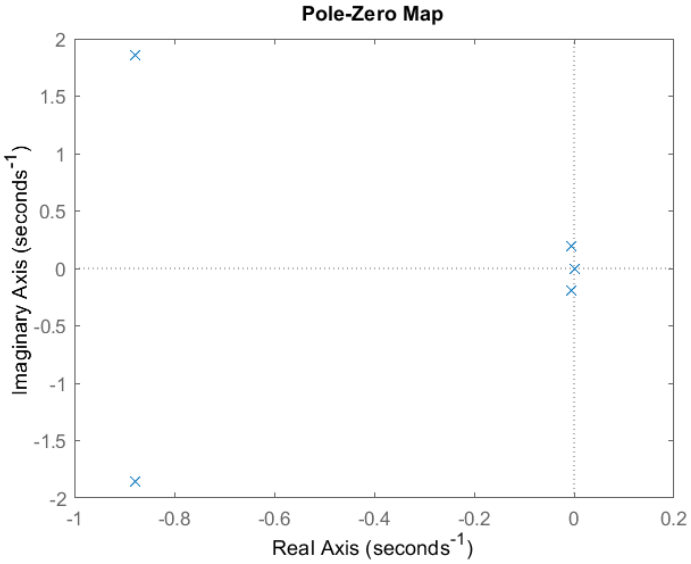

Figure 2.12: Plot of poles and zeros for longitudinal dynamics of the decoupled system.

The roll, dutch roll and spiral mode results from the lateral dynamics. The spiral mode is due to the pole close to the origin, the dutch roll from the complex poles near the imaginary axis and the roll mode from the most negative poles. Here the position of the roll poles indicated a stable, slightly oscillatory behaviour with the dutch roll poles indicating a much larger oscillatory response. The effect of the roll mode can be seen in figure 2.4 however the effects from the under-damped dutch roll mode result in the roll angle not stabilising as rapidly as it otherwise would. It is possible to observe the dutch roll effect in figures 2.8 and 2.9 however it is much harder to visualise the spiral mode from these plots.

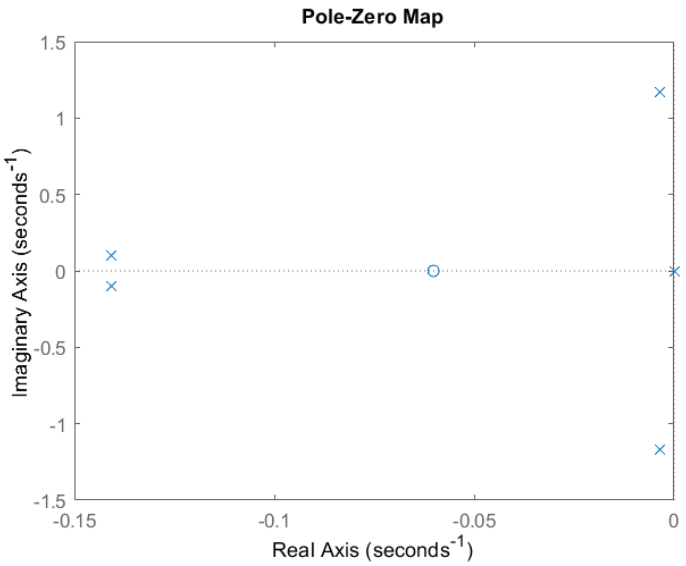

Figure 2.13: Plot of poles and zeros for lateral dynamics of the decoupled system.

3

Auto-pilot design

In this project, two different controllers were evaluated as a base for the autopilot. The two types of controllers used were PID and LQI controllers. The PID was selected as it is well understood and widely used in the aerospace industry [27]. Unlike optimal and model based-controllers such as the LQI, the PID is a classical controller which does not require a model of the plant in order to be tuned. The PID controller could instead be quickly tuned by simply adjusting the gains accordingly. On the other hand, LQI controllers require a linear plant model in order to calculate the gains of the controller [28]. Obtaining this model can prove challenging at times; however, once obtained, the tuning of these controllers is intuitive with a gain per state of the model. This can be desirable as it allows people without prior experience in the field of control theory to adjust the performance of the controllers and has the potential to make the controller developed in this project more usable and accessible. A model-based design approach has the additional benefit of relying on the plant model for the controller gains. When the plant model changes during the development of the aircraft, the LQI changes its gains based on the new plant model. This makes the LQI more suitable for the iterative development process in aerospace, giving more consistent results as the aircraft continues to evolve.

3.1 Structure

When it comes to controlling a 6-DOF model, there are several options available for the high-level control structure. For a system like an aircraft, which is characterised by slower dynamics controlled by relatively fast systems such as elevators, ailerons, and rudders, a cascaded control system is recommended [29]. A cascaded control structure is a multi-loop control structure where the output of one loop feeds into the input of the next loop. The inner-loop runs at a higher rate and ensures system stability, while the outer-loop runs at a slower rate and determines the reference for the inner-loop. For the autopilot, a structure similar to that used in commercial autopilots was chosen, consisting of a flight director, outer-loop, and inner-loop, see [30].

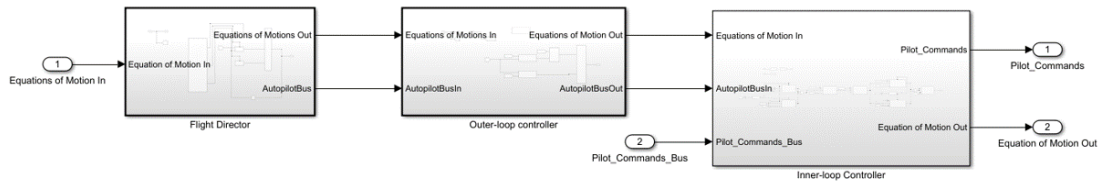

Figure 3.1: Example of a cascade control structure

3.1.1 Flight director

A flight director is a system that monitors the aircraft's states and determines what controllers are to be used and which trajectories are to be tracked. The flight director designed here utilised a state machine that could in real-time swap between various controllers and flight modes depending on the manoeuvre and the current state of the aircraft. This allowed for different states or parameters to be tracked in different manoeuvres as well as allowed for different weighting of gains between manoeuvres. For the manoeuvres covered in this project, a state machine was used, meaning that the flight director could sequentially swap modes once the specified conditions were met and were unable to swap back to previous modes. An example is the landing manoeuvre where the flight director swapped between 3 different controllers depending on where in the landing manoeuvre the aircraft currently was based on altitude. The flight director was not directly controlling the aircraft but was the source of information for the outer-loop and inner-loop.

3.1.2 Outer-loop

The outer-loop controller sat between the flight director and the inner-loop. This controller was responsible for generating a reference for the inner-loop based on the trajectory provided by the flight director. The outer-loop was responsible for the slower dynamics of the aircraft, such as heading and altitude, and outputted roll, pitch, yaw and true airspeed (TAS) references for the inner-loop. This controller ensured the aircraft correctly tracked the references provided by the flight director and compensated for disturbances such as wind or system failure.

3.1.3 Inner-loop

The inner-loop's primary purpose was to maintain stability and accurately track the desired reference commands provided by the outer-loop. It did this through the use of the aircraft's primary control surfaces such as the elevators, ailerons and rudder. Depending on which controllers were activated by the flight director, the inner-loop used different controllers for different references. The inner-loop received reference values such as roll, pitch, yaw and TAS from the outer-loop and flight director depending on the manoeuvre. The inner-loop was able to quickly respond to changes in the aircraft's dynamics, such as turbulence or sudden disturbances. It continuously adjusted the control inputs to ensure a smooth and stable flight by counteracting these fast changes.

3.2 Manoeuvres

To certify the aircraft for commercial flight it has to pass a certain set of manoeuvres required by the CS-25 standard [3]. In this thesis, the following manoeuvres were selected as they presented the most interesting challenges and covered both lateral and longitudinal motion while keeping the total number of manoeuvres to a minimum:

1. 30° bank-to-bank
2. Takeoff
3. Landing

The bank-to-bank manoeuvre requires the aircraft to roll from a 30° banked turn in one direction to a 30° banked turn in the opposite direction in less than 7 seconds. During this manoeuvre, the aircraft has to keep a gradient ascent where the airspeed should be between 1.3 stall speed (VSR) and maximum operating speed (VMO). This manoeuvre tests the aircraft in the lateral direction as well as the longitudinal tracking behaviour.

For takeoff, CS-25 requires that the aircraft is able to take off with the longitudinal trim set at any position within the normal trim range. At the time of designing this controller, the normal trim range had not yet been set and as such the aircraft was trimmed such that the aircraft would be in a stable climb with full thrust in the OEI case. This guaranteed that it would be possible to take off even if one motor failed during takeoff.

The landing manoeuvre is highly complex with the CS-25 listing multiple different scenarios and conditions that must be met. For the purpose of this project, it was decided that the objective of the landing manoeuvre would be to land with a vertical speed of approximately 3 ft/s and no more than 6 ft/s.

3.3 PID

PID is the most commonly used controller, with industries such as the process industry having more than 97% of all controllers being PIDs [27]. The PID is based on the principle of using 3 different terms based on the current and past error between the parameter that is being controlled and the reference. The proportional (P) term acts directly on the error between the reference signal and the current value and is the base of the controller. The integral term (I) is based on the cumulative error over time and is commonly used to remove steady-state error in the process. The final term is the derivative term (D) which acts on the rate of change of the error. This term is usually low-pass filtered as noise in the signal would cause the derivative term to become very large and unsettle the system.

The PID controller was present in both the inner and outer-loop of the control

system. In the outer-loop there were 3 different PID controllers, which were controlling the heading angle through roll angle, altitude through a pitch angle or vertical speed through a pitch angle. These roll and pitch reference angles were sent forward to the inner-loop controllers. Inside the inner-loop controller, the aircraft was controlled differently depending on which mode it was in.

The inner-loop controllers were created first as they were required for the outer-loop and flight director to have an effect. The controllers which handle longitudinal dynamics were created first with the pitch of the aircraft being controlled using thrust and the speed being controlled by the elevators. By increasing the thrust and keeping the elevators in trim condition the aircraft will naturally pitch up because of the added lift gained from a higher speed [7]. The speed of the aircraft can then be controlled by the elevators pitching up or down. For the lateral dynamics, the ailerons were used to roll the aircraft and the rudder for yawing the aircraft. These two controllers were tuned with the longitudinal controller active to keep a constant height while the roll and yaw controller was tuned. These PIDs were tuned using a mix of Ziegler-Nichols method [31] and manual tuning with trial and error to get a quick and representative result for each controller. The outer controller was created once the aircraft was stable and could follow pitch, roll and thrust references using the inner-loop. The outer-loop was tuned by requesting a heading angle or altitude angle and tuned accordingly with the same methods.

3.3.1 Roll manoeuvre

For the rolling manoeuvre, the airspeed was controlled by the elevator and the pitch angle was controlled by the thrust. This may feel counter-intuitive however this is common in aircraft that have lower power-to-weight ratios such as the aircraft used in this thesis [32]. During the manoeuvre, the rudder was able to solely work as a yaw damper, which minimised the yaw rate of the aircraft and prevented the aircraft from sliding sideways through the air [33]. The ailerons were then used to produce the rolling moment required to perform the manoeuvre.

3.3.2 Takeoff

The takeoff manoeuvre involved multiple modes with different controllers, where the variable being tracked changed throughout the manoeuvre. This required the flight director to change the controller and reference values during run-time for takeoff. The tracked variables and the controller switching conditions are described in table 3.1 below.

	Mode	Longitudinal	Lateral	Transition
1	Acceleration	θ	ϕ	TAS $\geq$ VR
2	Climb	TAS	ϕ	

Table 3.1: Reference states for takeoff using PID controllers

For the entire takeoff manoeuvre, the thrust command was set to the maximum.

This meant that the only control input in the longitudinal direction was the pitch command. In the lateral direction, the ailerons were used to control the roll angle and prevent the wings from striking the ground. During acceleration, the roll and pitch angle references were all set to 0 in order to keep the aircraft straight and level. Once the TAS exceeded rotation speed (VR) during the takeoff the flight director changed the references and controllers to track airspeed using the elevators. The lateral controller stayed the same, aiming to keep the wings level throughout the manoeuvre. The desired TAS reference comes from a desired climb angle generated by the outer-loop.

3.3.3 Landing

The full landing manoeuvre included three phases, namely the approach, flare and derotation phases. To achieve this, multiple modes were once again required and are detailed in table 3.2.

	Mode	Longitudinal	Lateral	Transition
1	Approach	TAS, Altitude	ϕ	Altitude $\leq$ flareHeight
2	Flare	TAS, Altitude	ϕ	Altitude $\leq$ touchDownHeight
3	Derotate	θ	ϕ	

Table 3.2: Reference states for landing using PID controllers

For this manoeuvre, the pitch command was used to control the speed and thrust used to control the altitude while in the lateral direction, the goal was to keep the wings level throughout the manoeuvre to prevent them hitting the ground. During the approach and flare phase, the reference speed was set to the approach speed while the altitude trajectory was created such that the vertical speed was 5 m/s during the approach and 1 m/s during the flare. The derotate phase was performed by reducing the thrust to 0 and tracking a pitch angle of 0 while applying the brakes.

3.4 LQI

The LQI controller is an optimal controller used to determine the optimal control gains for a given plant. The controller uses a cost index function to determine the optimal gain matrix. This cost function involves two weighting matrices, the Q and R matrix. The Q matrix is the weight matrix of the states and penalises any error in the state x, while the R matrix penalises actuator input u to create an energy-optimal controller. The LQI controller has been widely used in various applications, including aerospace, robotics, and control systems in general. It is particularly useful in controlling systems with integrators, as it allows for the removal of steady-state errors. Compared to the PID the LQI did not need an outer-loop and could receive the references straight into the inner-loop.

Given a system in standard state space form with the cost function:

$$J = \int_0^\infty (x^T Q x + u^T R u) \tag{3.1}$$

the optimal controller which minimises the cost function is:

$$u = -Kx \tag{3.2}$$

where the gain matrix K is defined as:

$$K = R^{-1}B^{T}P \tag{3.3}$$

and with P obtained by solving the time-continuous Riccati equation [34].

$$A^{T}P + PA - PBR^{-1}B^{T}P + Q = 0 \tag{3.4}$$

By using the decoupled state space matrix a gain matrix K could be found for the lateral dynamics and one for longitudinal dynamics by using the Matlab command `lqr(system,Q,R)` where the Q and R were individually chosen depending on the mode the aircraft was flying in.

During flight, the system may be affected by constant disturbances from wind or loss of power. This constant disturbance offset could be dealt with by integrating the error between the output and the reference signal.

$$\dot{x}_i = r - y \tag{3.5}$$

Using this new variable $\dot{x}_i$ the states of the state space system can be augmented in the following format.

$$\dot{x}_a = \begin{bmatrix} \dot{x} \\ \dot{x}_i \end{bmatrix} = \begin{bmatrix} A & 0 \\ -C & 0 \end{bmatrix} x_a + \begin{bmatrix} B \\ 0 \end{bmatrix} u \tag{3.6}$$

This gives a state space system that includes the new integral state $\dot{x}_i$ and will cancel out steady state disturbances.

In order to calculate gain matrices defined in eq 3.2 a process was set up to make it as automated as possible. The linearization process described in section 2.3 was set up to produce the decoupled state space model, all that was required was to create a function that would take the decoupled state space systems, obtain the correct integral states and weighting matrices based on which manoeuvre was selected and then call the built-in MATLAB command `lqr(system,Q,R)` with the augmented state space model described in equation 3.6.

3.4.1 Rolling manoeuvre

When performing the rolling manoeuvre using LQI only two controllers were required as opposed to the PID version which used 4 controllers. The two controllers used by the LQI are for the longitudinal and the lateral-directional motion, using their corresponding decoupled state-space equations as the plant models. The aircraft was trimmed for a given flight path angle needed to perform the ascent during the manoeuvre. Similar to the PID the flight director sent a reference roll angle to the lateral-directional controller to perform the banking turn. For the longitudinal

control, the controller received both TAS and height as the reference to follow.

The Q and R matrix which forms the LQI controller were weighted differently depending on which manoeuvre was performed and what the integral states were. In the rolling manoeuvre, there was an emphasis on weighting the inputs to prevent the control surfaces from saturating. In addition to this, the Q matrix in the lateral direction had higher weightings on the roll angle compared to the other states to make sure the correct angle was reached.

Mode	Longitudinal	Lateral
Roll mode	Height, Airspeed	Roll angle

Table 3.3: Integral states for rolling manouvre

3.4.2 Takeoff

The takeoff manoeuvre using LQI was done in a very similar way as the PID with some changes to the tracked states, as described in table 3.4. Instead of only using the rudder as a yaw damper, it was used to help keep the aircraft going in a straight line. This was easily possible as instead of having to tune individual PID controllers, the LQI handled the coupling between the rudder and ailerons.

	Mode	Longitudinal	Lateral	Transition
1	Acceleration	θ	ϕ, ψ	TAS $\geq$ VR
2	Climb	TAS	ψ	

Table 3.4: Integral states for takeoff

Much like for the PID controller, the thrust was kept at maximum for the entire manoeuvre. Similarly, during acceleration the roll, pitch and yaw references were all kept at 0 and, once the mode changed to climb, the reference TAS was set to the target climb speed. In this case, once the aircraft left the runway and started climbing the roll tracking was removed allowing the aircraft to roll and counter the effect of any crosswinds.

During acceleration, the roll and yaw states were weighted the most in the tuning matrix as it was critical that the aircraft remain straight and level to prevent the wings from striking the ground. The pitch rate state was given the largest weighting in the longitudinal direction which gave a dampening effect on pitch. This was done to quickly correct for any pitching moment imparted from the ground. During the climb phase a greater weighting was placed on the yaw state and less on roll as the main goal was to continue flying straight, especially if any lateral disturbances were experienced. A larger weighting was also placed on the pitch state as it became important to maintain the climb angle. The weighting on the TAS integral state was kept relatively small such that the aircraft would not do drastic pitching manoeuvres to rapidly acquire the desired airspeed.

Although the previous method was capable of performing the takeoff manoeuvre it was desirable from an aircraft performance perspective for the TAS to never decrease. To achieve this a number of additional modes were required, detailed in table 3.5.

	modes	Longitudinal	Lateral	Transition
1	Acceleration	θ	ϕ, ψ	TAS $\geq$ VR
2	Rotate	θ	ϕ, ψ	TAS $\geq$ 95% climb speed
3	Transition	θ, TAS	ϕ, ψ	TAS $\geq$ 99.9% climb speed
4	Climb	TAS	ψ	

Table 3.5: Integral states for takeoff with performance requirements

Similar to the previous takeoff method, the thrust was set to the maximum throughout the manoeuvre. The acceleration phase was also the same with the reference roll, pitch and yaw set to 0. During the rotation mode, the reference pitch was set to 98% of the climb angle. This caused the aircraft to rotate and begin climbing while continuing to accelerate. Once the TAS got close to the final climb speed only TAS and ψ were tracked. When swapping from tracking the climb angle to tracking the desired airspeed a large step in the control action was observed as the controller attempted to reach the target climb speed. This resulted in the aircraft pitching down and overshooting the desired TAS. The solution to this was adding the transition stage which implemented bump-less switching.

Bump-less switching is a method used to mitigate large steps in controller outputs when switching between controllers [35]. For this case, it was decided to use the TAS as the scheduling variable. The transition between the controller tracking θ and the controller tracking TAS was done as the TAS went from 95% climb speed to 100% climb speed. As a result instead of the structure seen in equation 3.2 the control output had the following form.

$$u = (1 - \zeta(TAS))(-K_{theta}x) + \zeta(TAS)(-K_{TAS}x) \quad \zeta(TAS) \in [0 \;\; 1] \tag{3.7}$$

Where ζ is a function of TAS

$$\zeta(TAS) = \frac{TAS - 0.95 climbSpeed}{0.05 climbSpeed} \tag{3.8}$$

This resulted in the θ controller keeping the nose up and slowing down the transition while the TAS controller slowly gained more and more authority and guided the TAS towards the final target value. Once the TAS got close to the target climb speed the bump-less switching could be disabled and only the TAS tracked.

3.4.3 Landing

For the landing manoeuvre, some changes were made in the tracked states when compared to the PID implementation. Once again, the rudder was allowed to op-

erate as more than a yaw damper however the sink speed was tracked instead of a height trajectory to improve robustness from vertical disturbances.

	Mode	Longitudinal	Lateral	Transition
1	Approach	TAS, Sink speed	ϕ	Altitude $\leq$ flareHeight
2	Flare	TAS, Sink speed	ϕ	Altitude $\leq$ touchDownHeight
3	Derotate	θ	ϕ	

Table 3.6: Reference states for landing using LQI controller

The reference TAS was the approach speed with the reference sink speed switching from -5 m/s to -1 m/s from the approach to the landing phase. The derotate phase once again reduced the thrust to 0, tracked a pitch angle of 0 and applied the brakes.

During the approach and flare the same controller and weightings were used with only the reference changing. For this phase the largest weighting was put on the yaw angle and lateral velocity as it was critical the aircraft was not moving sideways at touchdown otherwise the aircraft risked rolling. In the longitudinal direction, the largest weighting was placed on the integral states as maintaining the correct sink speed and approach speed was needed in order to achieve a gentle touchdown. During the derotation, a large emphasis was put on roll to prevent any rolling from happening after touchdown. This was especially important when experiencing lateral disturbances. Similar to the acceleration phase of takeoff, a large weighting was put on the pitch rate to have a dampening effect and combat potentially large moments caused by the landing gear on the runway.

3.5 Envelope testing

The position of the COG of an aircraft and the total weight of the aircraft can have an impact on the aircraft's flight qualities and behaviour [36]. Depending on how the aircraft is loaded and how much fuel it is carrying, the COG and total weight varies. The limits of these variations are commonly described in a CG envelope and are specific to each aircraft. In the example shown in figure 3.2, the maximum and minimum acceptable weight depending on the position of the COG can be seen.

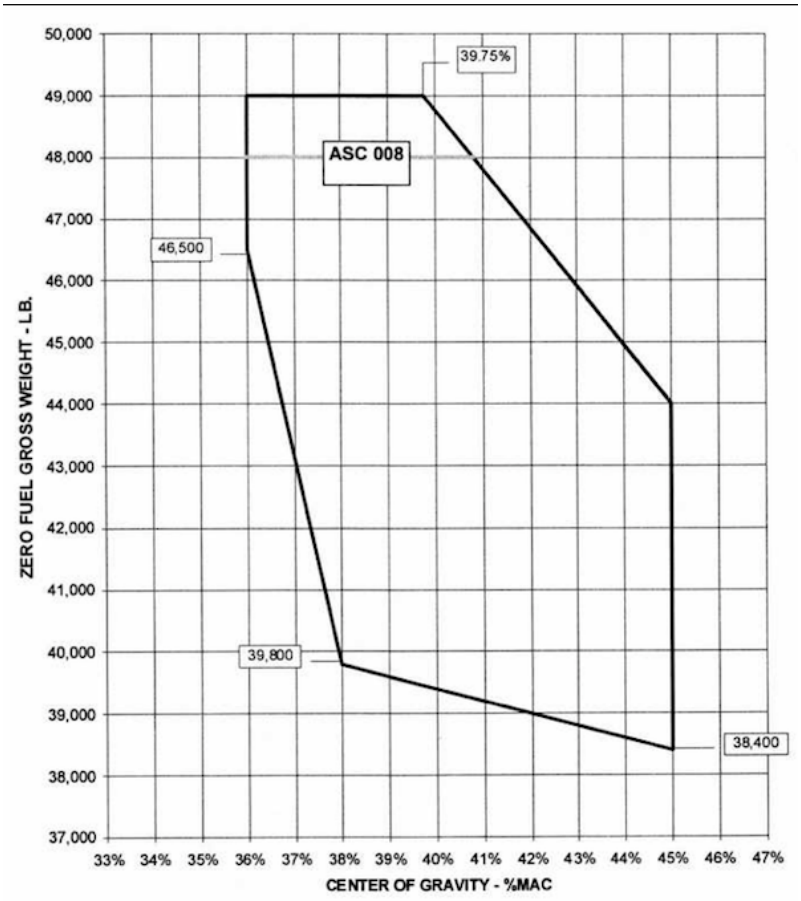

Figure 3.2: CG envelope for a Gulfstream 450 [36]

Although the weight envelope represents a continuous region, the main points of interest are those on the perimeter of the envelope, and specifically those on vertices. These points represent the most extreme cases the aircraft is expected to encounter. For the ES-30 this resulted in 11 points, described in table 3.7, at which it was interesting to observe the aircraft performance.

Acronym	Name
mrw fwd	Maximum Ramp Weight forward
mrw aft	Maximum Ramp Weight aft
mtow fwd	Maximum takeoff weight forward
mtow aft	Maximum takeoff weight aft
mlw fwd	Maximum landing weight forward
mlw aft	Maximum landing weight aft
mzfw fwd	Maximum design zero fuel weight forward
mzfw aft	Maximum design zero fuel weight aft
mow fwd	Minimum operating weight forward
mow aft	Minimum operating weight aft
min aft	Minimum weight aft

Table 3.7: Reference states for landing using LQI controller

It was important to be able to perform the manoeuvres at all of these points and to be able to perform these tests without the need to manually change the COG case and restart the simulation for each point. To this end, a MATLAB script was created where the user could select the desired manoeuvre at the beginning and then the script would automatically step through all COG cases. In order to achieve this it was important to set up the simulation and the initialisation of its variables such that they could be changed programmatically. It was also necessary to be able to store the output of the simulation for post-processing. Once all the simulations had finished running it was desirable for the data to be automatically plotted. To achieve this a set of functions were created that were capable of plotting the output data. It was then possible to define the selection of plots desired for each manoeuvre such that the final set of plots was determined based on the manoeuvre the user selected at the beginning. A post-processing function was also created that would analyse the data from the simulations and indicate points where hard limits were exceeded or where an event happened that should be further investigated by the user. This functionality was not fully developed as other tasks took priority however it was able to notify the user and provide time stops for the following events:

1. Exceeding maximum g-force level
2. Exceeding stall angle
3. Saturation of control inputs
4. Exceeding minimum altitude

This analysis and detection was done by running through the simulation data and looking for points that exceeded the limits defined. Any failures were then saved in a list specifying the manoeuvre, the COG case, the type of failure and the time

at which it occurred. If any failures occurred, the total number would be displayed to the user with the full list stored in the event that the user wanted to see the details. Avoiding automatically showing the list prevented cluttering the workspace as it was often unnecessary to view the detailed list.

3.6 Failures

As well as forming a part of many of the CS-25 requirements [3], it is often interesting to evaluate the performance of an aircraft when one or more failures occur. For this aircraft, the most interesting failure was that of a motor (the OEI case) as well as a failure which caused the range of motion of the control surfaces to be reduced. To achieve this a set of functions was created such that before running any simulation it was possible to easily define which motor to disable or which control surface should have a limited range and how large that range should be. The motor failure functions made use of the existing functionality in the non-linear model to set failure flags and simply made it possible to define these flags programmatically. To limit the control surface ranges, parameters used in the flight controls block to determine the maximum and minimum deflection were altered to reflect the desired ranges. Finally, by ensuring the default condition was stored, the failures could be easily reset. As such it was possible to automatically disable and re-enable the failure before and after trimming if required. This was necessary for the envelope testing in situations where the aircraft needed to be trimmed without the failure present.

3.6.1 Motor failure

The failure of a motor presented two main challenges. The first was during takeoff as the total amount of thrust available was lower than with all four motors operable. This demanded a different reference for the climb angle depending on whether a failure was present or not. To obtain the reference climb angle the aircraft was trimmed twice, once for the OEI case and once for the all engines operable (AEO) case. Then, depending on whether a failure was detected or not the flight director would change the reference pitch angle accordingly. The second main challenge was during landing as the yaw moment caused by the thrust imbalance could cause the aircraft to touch down with a yaw angle and lateral velocity large enough to cause the aircraft to tip over. This could however be fixed by applying a strong weighting to these states in the tuning matrices.

3.7 Disturbance

Some of the requirements such as L1 FSS 34 [3] require the aircraft to be able to take off with a crosswind of 30 knots and with no more crab angle than 4° degrees. This type of test required the simulation to involve disturbances such as wind. There are different types of wind models and the ones covered in this thesis are steady state

wind, wind shear model wind and Dryden turbulence model. These type of winds covers most of the models that could be needed to get an accurate model of how the aircraft would perform a takeoff with a crosswind.

The wind disturbance was integrated into the envelope testing in such a way that the type of wind, direction and speed were very easily modified before the testing starts. This made testing of different wind directions on each envelope point very easy and it could later be evaluated on how the aircraft handles different directions and speeds.

3.7.1 Steady-state wind

The steady-state wind was the most basic wind model and also the most unrealistic. The wind held a constant speed and direction which was decided using a variable for speed and one vector for direction in x,y and z coordinates. These wind forces were then directly applied to the aerodynamics of the model and could cause very different behaviours. This wind direction was in the global coordinate system which meant that during a banking manoeuvre where the heading of the aircraft constantly changed the wind direction acting on the aircraft changed as well.

3.7.2 Wind shear model

The wind shear model, also known as wind gradient, was a mathematical wind model which was based on an implementation from [37]. There were two types of wind shear where one was a changing wind speed depending on the altitude and the other was a horizontal wind shear model where wind speed was dependent on the horizontal movement of the aircraft.

How the wind was affected at different heights was calculated using the following formula where there was measured reference wind speed at a certain reference height and from this, the expected wind speeds at other heights could be calculated depending on the terrain.

Variable	Description
V_1	Wind speed at height h_1 in m/s
V_2	Wind speed at height h_2 in m/s
h_1	Reference altitude in meters
h_2	Current altitude in meters
v_0	Roughness length

$$V_2 = V_1 \frac{\ln(\frac{h_2}{z_0})}{\ln(\frac{h_1}{z_0})} \tag{3.9}$$

The coefficient z_0 is the roughness length which depends on the different types of areas where the measurement is taken. Table 3.8 shows how z_0 changes depending

on the condition of the environment. The roughness class of the tests performed in this thesis was set at a roughness class of 0.5 which corresponds to most airports.

Roughness class	Roughness length z_0	Land cover types
0	0.0002 m	Water surfaces: seas and lakes
0.5	0.0024 m	Open terrain with smooth surface, e.g. concrete, airport runways, mown grass etc.
1	0.03 m	Open agricultural land without fences and hedges; maybe some far apart buildings and very gentle hills
1.5	0.055 m	Agricultural land with a few buildings and 8 m high hedges separated by more than 1 km
2	0.1 m	Agricultural land with a few buildings and 8 m high hedges separated by approx. 500 m
2.5	0.2 m	Agricultural land with many trees, bushes and plants, or 8 m high hedges separated by approx. 250 m
3	0.4 m	Towns, villages, agricultural land with many or high hedges, forests and very rough and uneven terrain
3.5	0.6 m	Large towns with high buildings
4	1.6 m	Large cities with high buildings and skyscrapers

Table 3.8: Table showing roughness classes, roughness length Z_0, and land cover types

Wind shear and constant wind models do not include any type of turbulent disturbance as it only uses pre-determined velocities and directions. If it is of interest to represent the real-life scenario of crosswind wind gusts then the Dryden model would be used as it is one of the most commonly used continuous turbulence models [38] and is accepted by the United States Department of Defence in their aircraft design development. The model uses a mathematical model to simulate turbulence by combining a variety of frequencies and amplitudes to the wind gusts acting on the aircraft. Each gust is modelled separately with its own intensity and duration.

4
Results

Testing of the designed controllers and manoeuvres was performed using the envelope testing described in section 3.5. All tests were performed with the controllers in their best-performing state after all tuning was complete. Aside from the variations described in the previous chapter, all references were kept the same between the controller tests.

4.1 Ideal conditions

The first set of tests done was on a system with no disturbances or failures. Although many of the manoeuvres required by the CS-25 include disturbances and/or failures, there are also many which don't require either. This ideal case was additionally useful in gaining insight into how the controller and aircraft perform in perfect conditions making it possible to identify behaviour caused by the failures or disturbances. All manoeuvres were performed with both the LQI and PID controllers.

4.1.1 Roll manoeuvre

The roll manoeuvre, explained in section 3.2, required the aircraft to reach a 30° bank angle and then, in under 7 seconds, roll 60° to reach a 30° bank angle in the opposite direction while climbing.

During the PID roll manoeuvre all the points successfully made it to the required bank angle within the time limit, as can be seen in figure 4.1, but with oscillations at the end of the manoeuvre. The altitude was tracked with minimal deviation and, most importantly, the desired climb rate was met throughout the rolling manoeuvre. The LQI controller follows the rolling trajectory more smoothly than the PID with no overshoot. The LQI begins rolling slightly slower than the PID but quickly hits the required roll rate to perform the manoeuvre in time. Compared to the PID there is no longer any oscillatory behaviour at the final trajectory and the roll angle settles at the desired angle more quicker. The amount of side slip seen from the PID controller spikes during the rolling moments however it does stabilise once the aircraft stops rolling. The LQI maintains a much lower amount of side slip angle throughout.

The roll and yaw commands from the PID show relatively similar peak values compared to the LQI however the LQI commands show fewer sharp changes and exhibit

more of a single large command at the time of rolling before settling to smaller values once more. Both controllers are able to meet the required roll rate without using more than 30% of the maximum roll command.

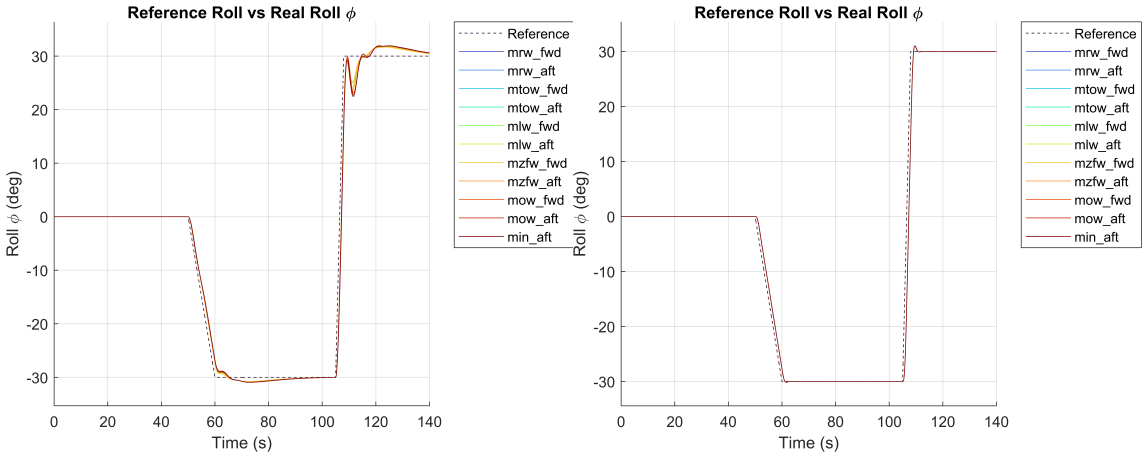

(a) PID **(b)** LQI

Figure 4.1: Roll plot for rolling manoeuvre while climbing using PID (4.1a) and LQI (4.1b) controllers

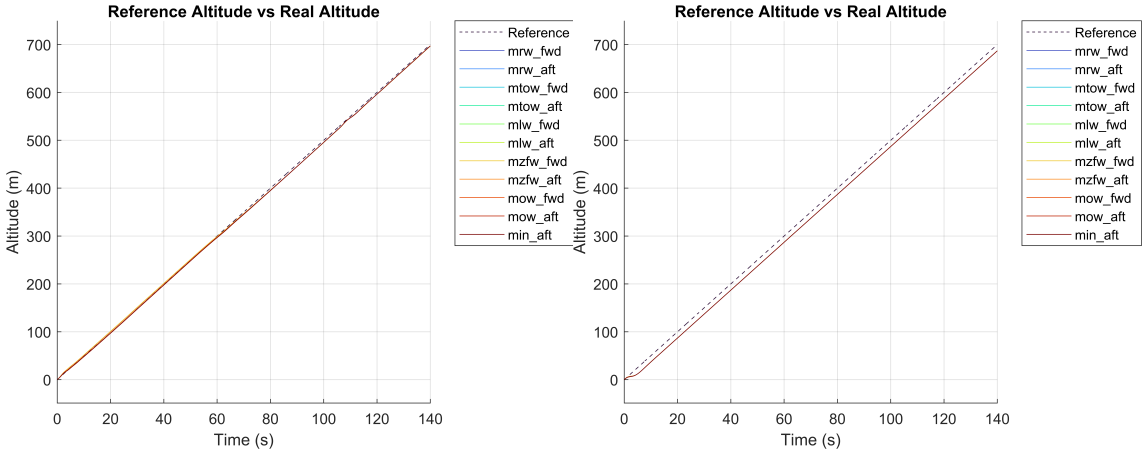

(a) PID **(b)** LQI

Figure 4.2: Altitude plot for rolling manoeuvre while climbing using PID (4.2a) and LQI (4.2b) controllers

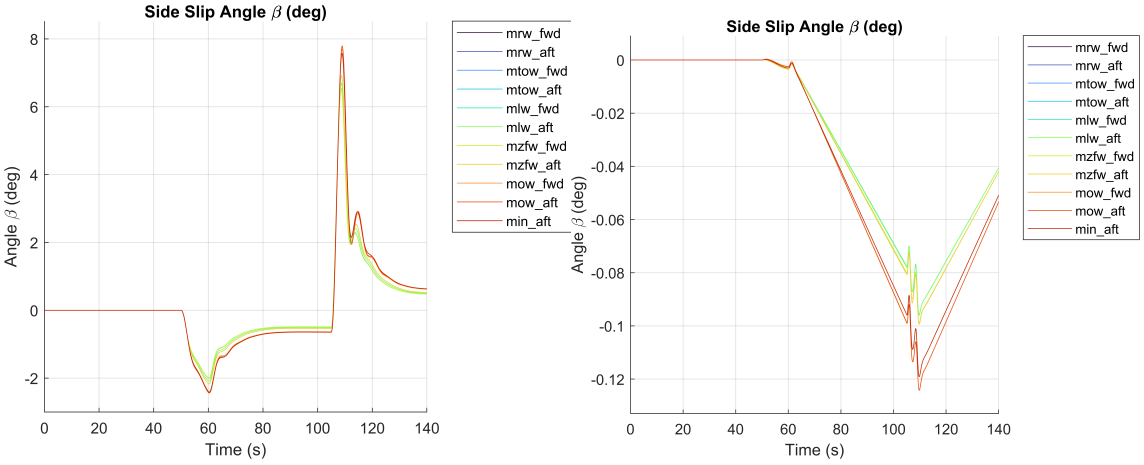

(a) PID **(b)** LQI

Figure 4.3: Side slip plot for rolling manoeuvre while climbing using PID (4.3a) and LQI (4.3b) controllers

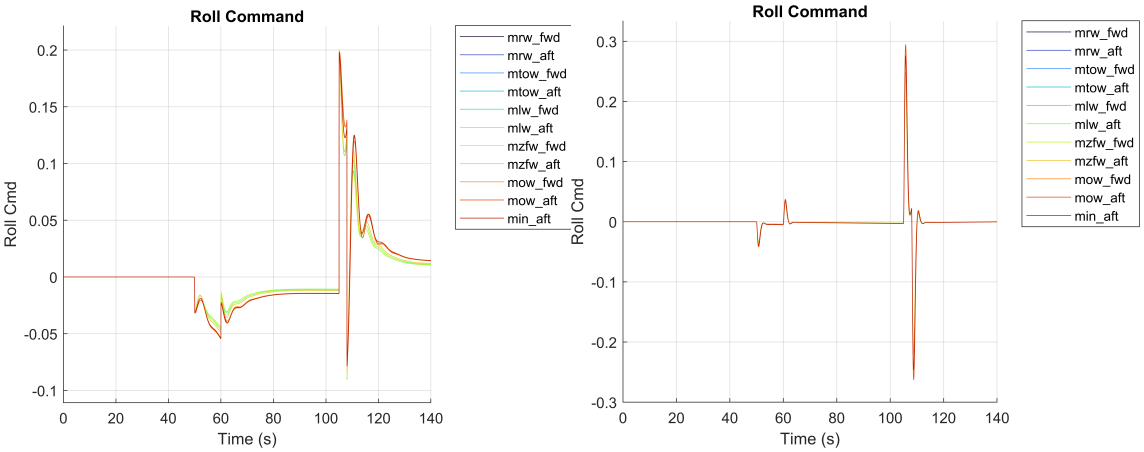

(a) PID **(b)** LQI

Figure 4.4: Roll command plot for rolling manoeuvre while climbing using PID (4.4a) and LQI (4.4b) controllers

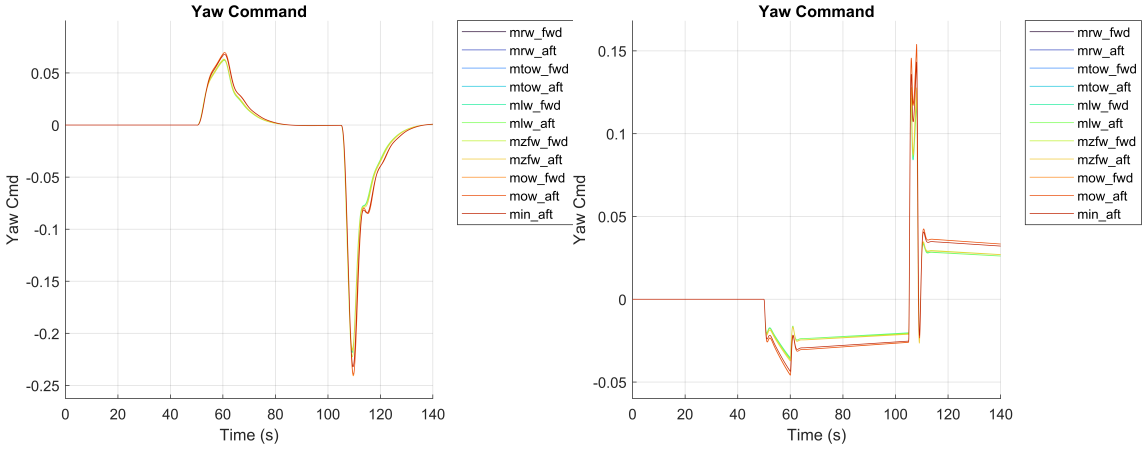

(a) PID **(b)** LQI

Figure 4.5: Yaw command plot for rolling manoeuvre while climbing using PID (4.5a) and LQI (4.5b) controllers

4.1.2 Takeoff

The takeoff manoeuvre has different climb rates and airspeeds for each COG case. This is because the total mass of the aircraft affects the resulting stall speed and therefore the desired airspeed and climb angle. This effect can be most easily seen in figures 4.6 and 4.7 where the altitude gradient and final TAS values are different for each case.

The PID controller shows an overshoot and some under-damped oscillations in the airspeed for all envelope points. The LQI shows a similar behaviour but with fewer oscillations and a longer settling time compared to the PID. Comparing the pitch angle of the PID and LQI in figure 4.8 it can be seen that the LQI manages to take off with a smaller peak pitch angle. As a result of this pitch peak, it can be seen that the stall angles for all but 2 envelope points in the PID case reach an angle of attack of higher than 10 degrees compared to the LQI where only 2 cases reach above 10 degrees. The pitch command seen in figure 4.10 shows the PID to be more oscillatory, especially for the low-weight cases. The LQI has much larger amounts of control action while still on the ground however when pitching up and climbing it lessens and is generally lower than the PID.

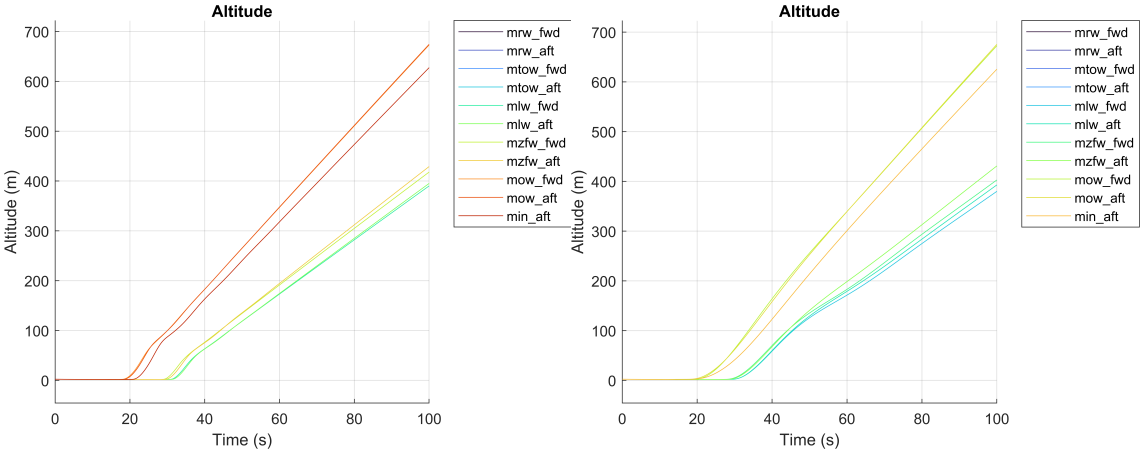

(a) PID **(b)** LQI

Figure 4.6: Altitude plot for takeoff manoeuvre using PID (4.6a) and LQI (4.6b) controllers

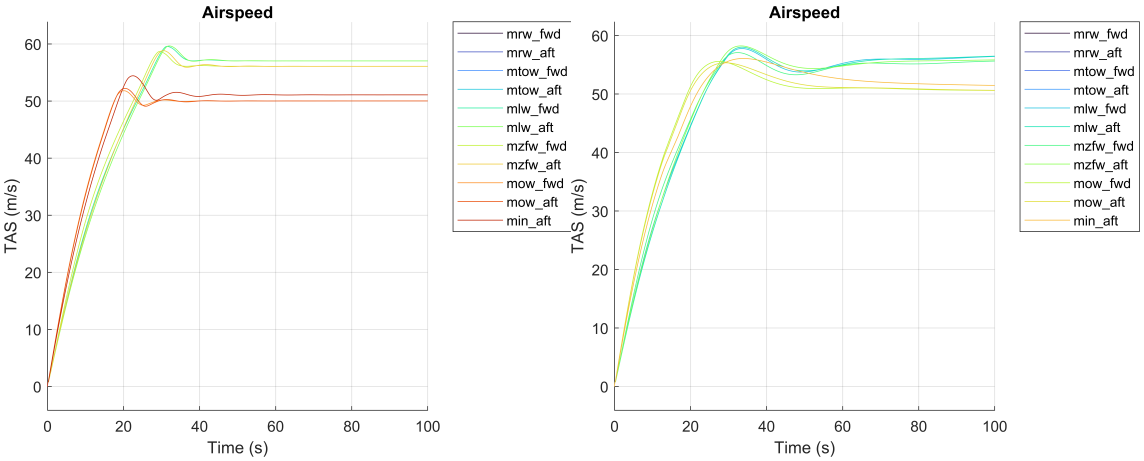

(a) PID **(b)** LQI

Figure 4.7: Airspeed plot for takeoff manoeuvre using PID (4.7a) and LQI (4.7b) controllers

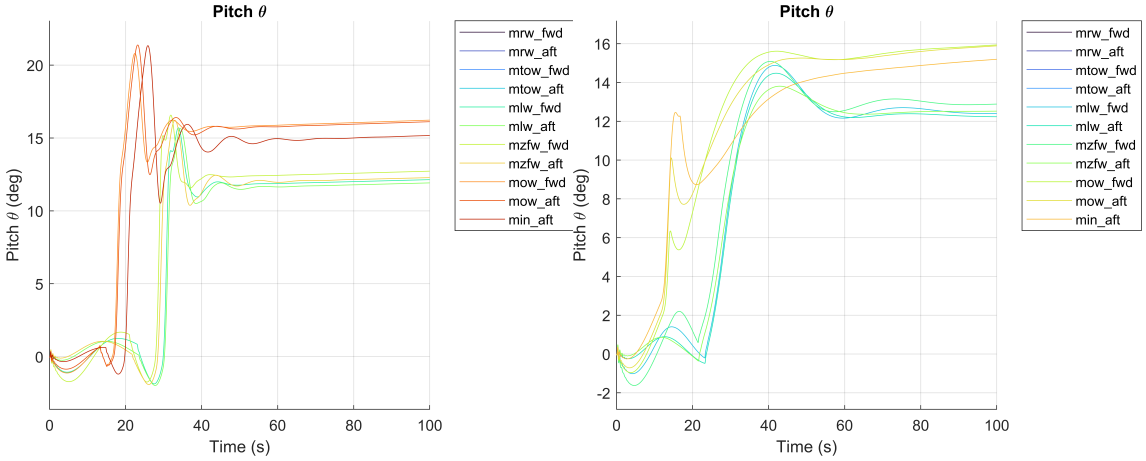

(a) PID **(b)** LQI

Figure 4.8: Pitch angle plot for takeoff manoeuvre using PID (4.8a) and LQI (4.8b) controllers

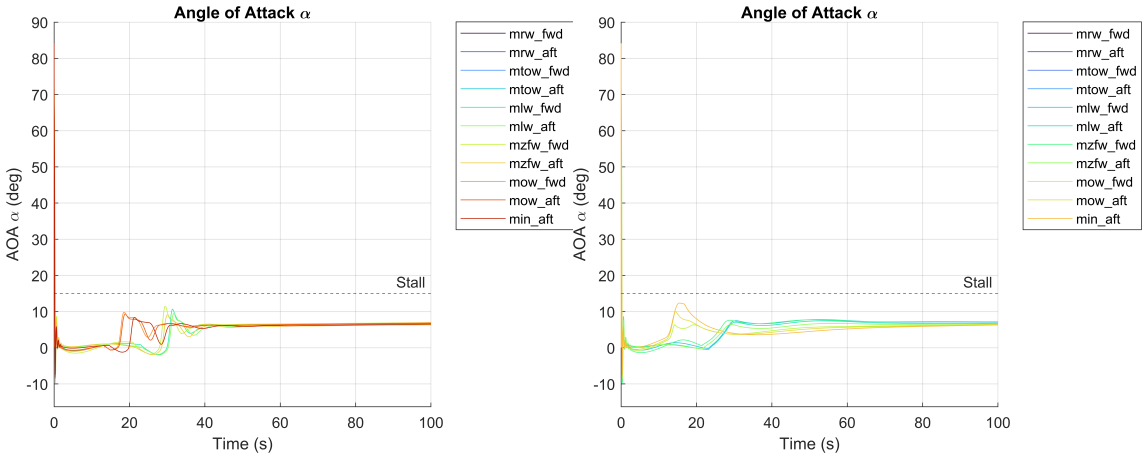

(a) PID **(b)** LQI

Figure 4.9: Angle of attack plot for takeoff manoeuvre using PID (4.9a) and LQI (4.9b) controllers

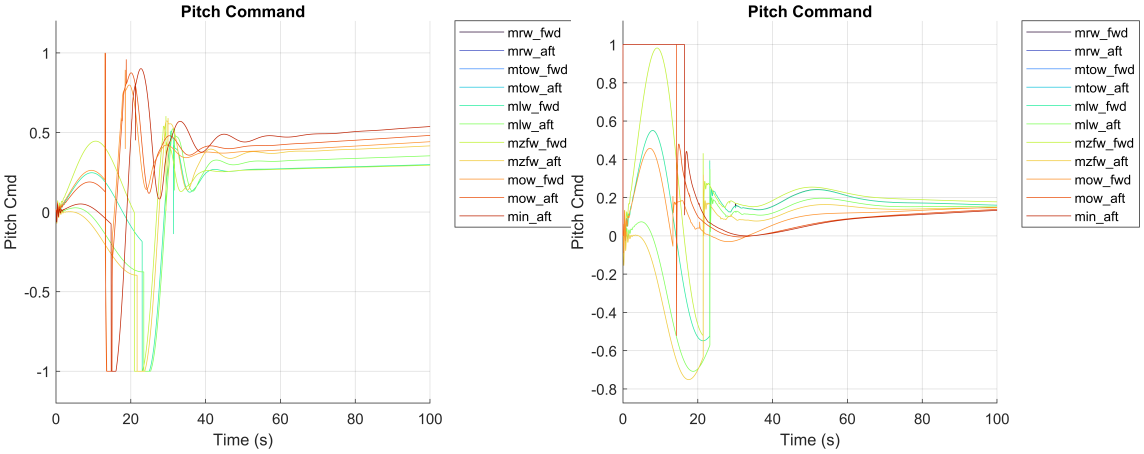

(a) PID **(b)** LQI

Figure 4.10: Pitch command plot for takeoff manoeuvre using PID (4.10a) and LQI (4.10b) controllers

4.1.2.1 Improved takeoff

The improved takeoff shows less drastic changes in the pitch rate, as seen in figure 4.14, and a smoother pitch which would result in a smoother ride during takeoff. The angle of attack is more consistent between COG case with the highest value being lower than that experienced in the original LQI case. The airspeed for the improved case has a positive gradient for almost all cases however the airspeed does decrease slightly for the min_{aft} case. The original LQI shows more significant decreases in airspeed, however, it was not attempting to prevent this. The pitch command for the improved takeoff seen in figure 4.10b is less smooth than the original, spiking once to rapidly acquire the initial climb angle and a second time to reach the final climb angle.

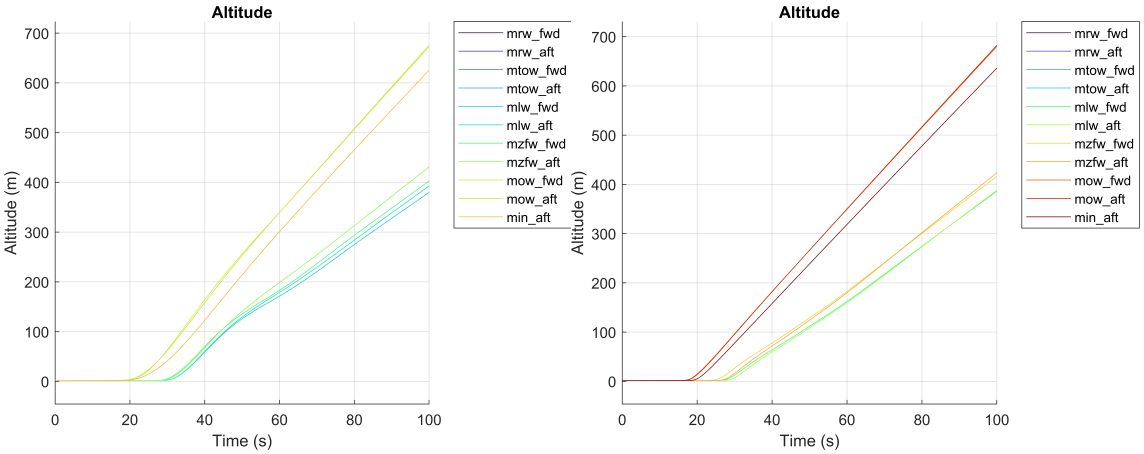

(a) LQI **(b)** Improved LQI

Figure 4.11: Altitude plot for takeoff manoeuvre using LQI (4.11a) and improved LQI (4.11b) controllers

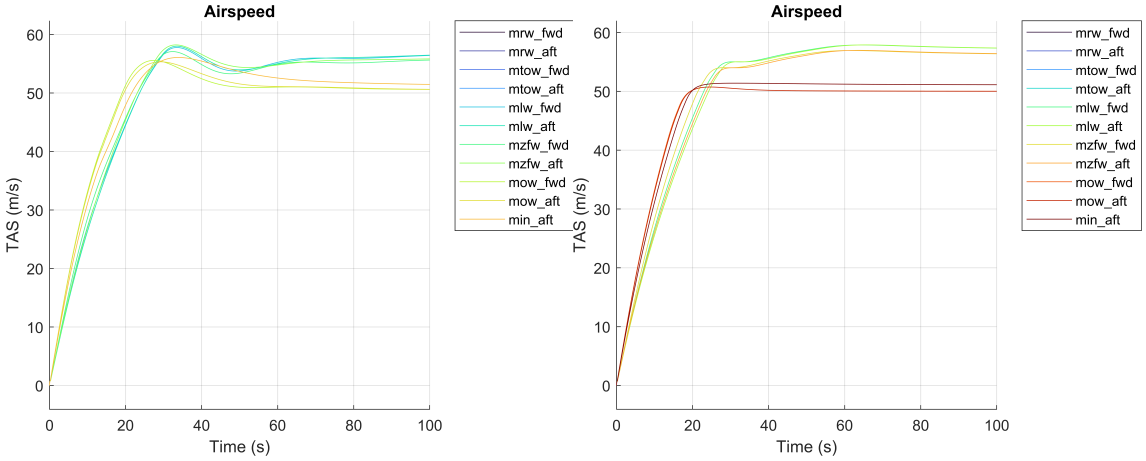

(a) LQI **(b)** Improved LQI

Figure 4.12: Airspeed plot for Takeoff manoeuvre using LQI (4.12a) and improved LQI (4.12b) controllers

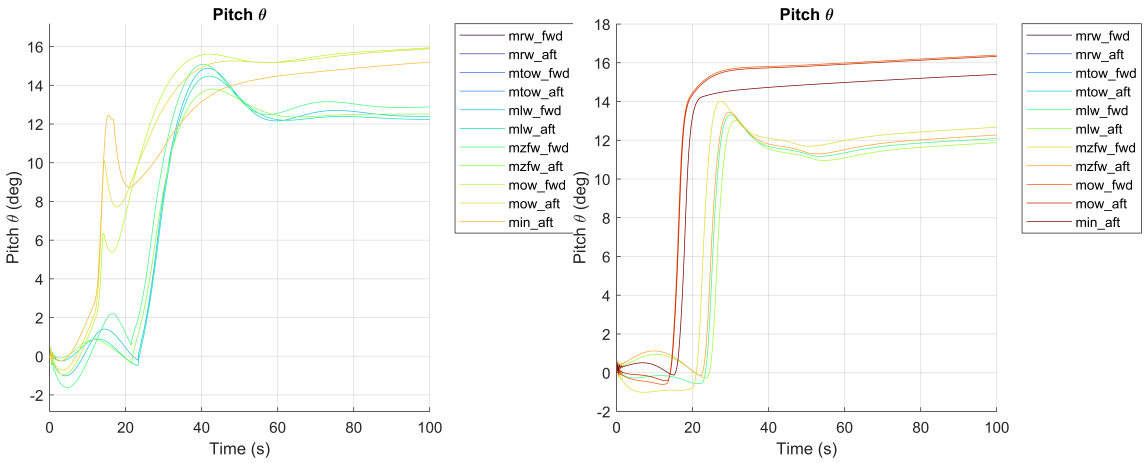

(a) LQI **(b)** Improved LQI

Figure 4.13: Pitch angle plot for takeoff manoeuvre using LQI (4.13a) and improved LQI (4.13b) controllers

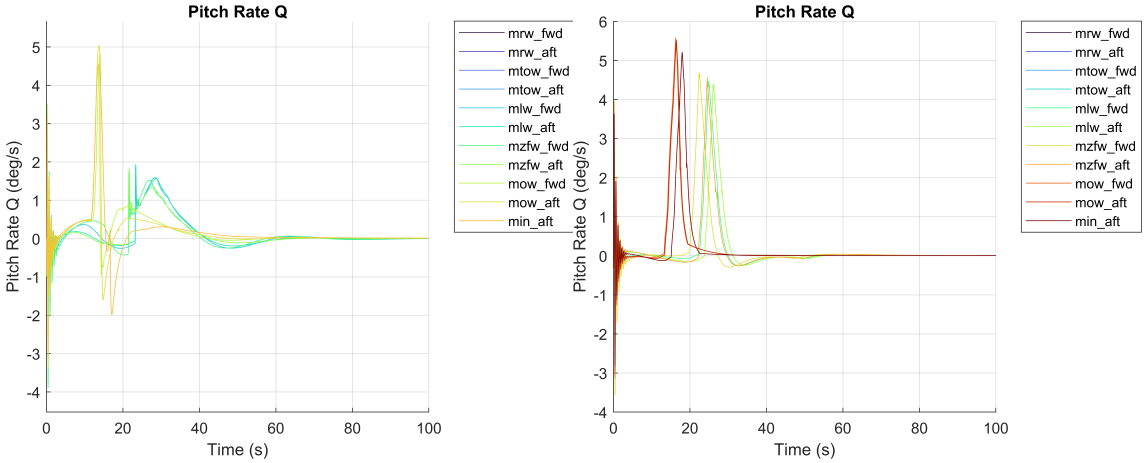

(a) LQI **(b)** Improved LQI

Figure 4.14: Pitch rate plot for takeoff manoeuvre using LQI (4.14a) and improved LQI (4.14b) controllers

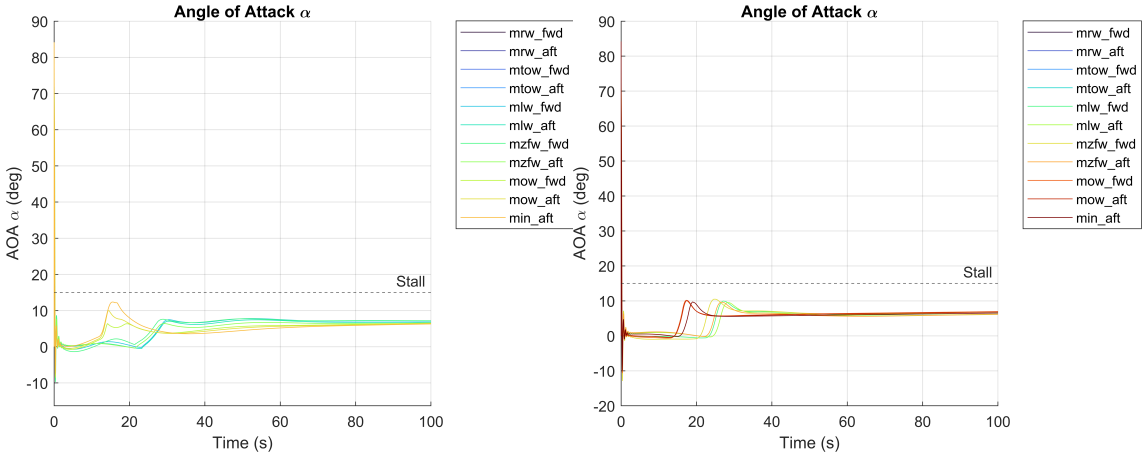

(a) LQI **(b)** Improved LQI

Figure 4.15: Angle of attack plot for takeoff manoeuvre using LQI (4.15a) and improved LQI (4.15b) controllers

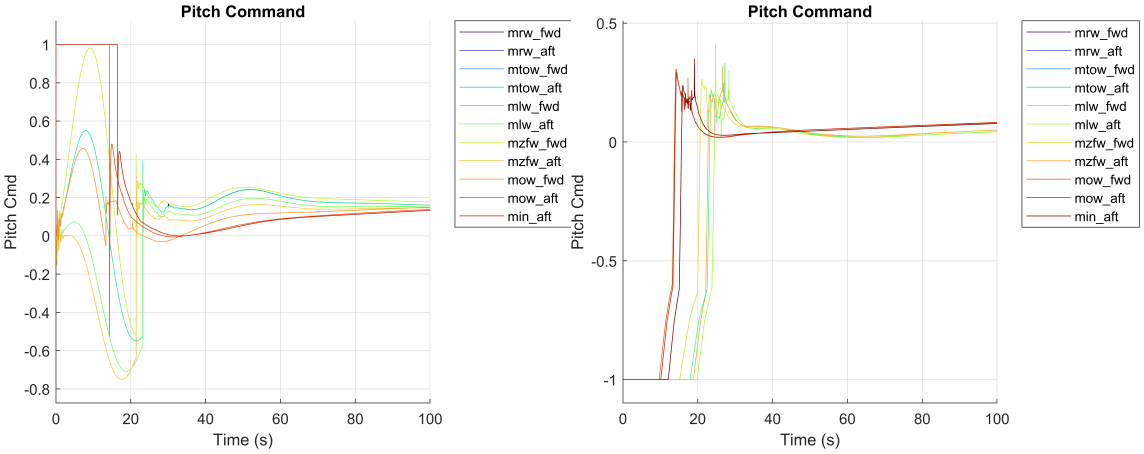

(a) LQI **(b)** Improved LQI

Figure 4.16: Pitch command plot for takeoff manoeuvre using LQI (4.16a) and improved LQI (4.16b) controllers

4.1.3 Landing

The time up to 90 seconds represents the descent, with the flare occurring between 90 seconds and 110 seconds. After touchdown, at around 110 seconds, the derotation occurs. These modes can be best visualised by looking at the pitch plots in figure 4.18. Throughout this manoeuvre the LQI controller has a much smoother control of the pitch angle with the pitch rate not having the directional changes seen in the PID pitch rate (figure 4.19a). The vertical speed for both controllers is at the desired value at touchdown, with the LQI acquiring the lower value quicker during the flare. The control action between the two cases is relatively similar, with the PID case showing slightly more spikes than the LQI at the start of the flare and at the moment of touchdown. In both cases, the vertical speed is at the desired level and the manoeuvre would be considered successful in both cases.

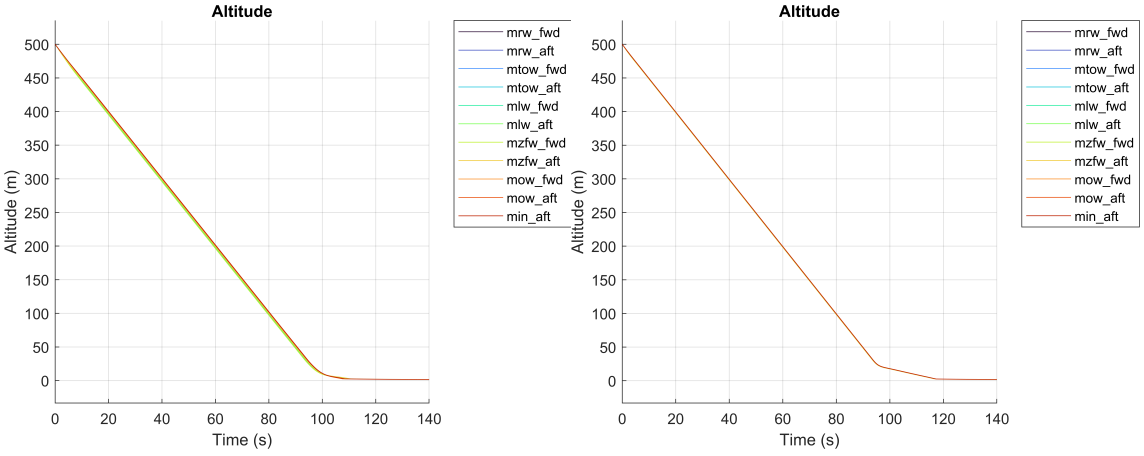

(a) PID **(b)** LQI

Figure 4.17: Altitude plot for landing manoeuvre using PID (4.17a) and LQI (4.17b) controllers

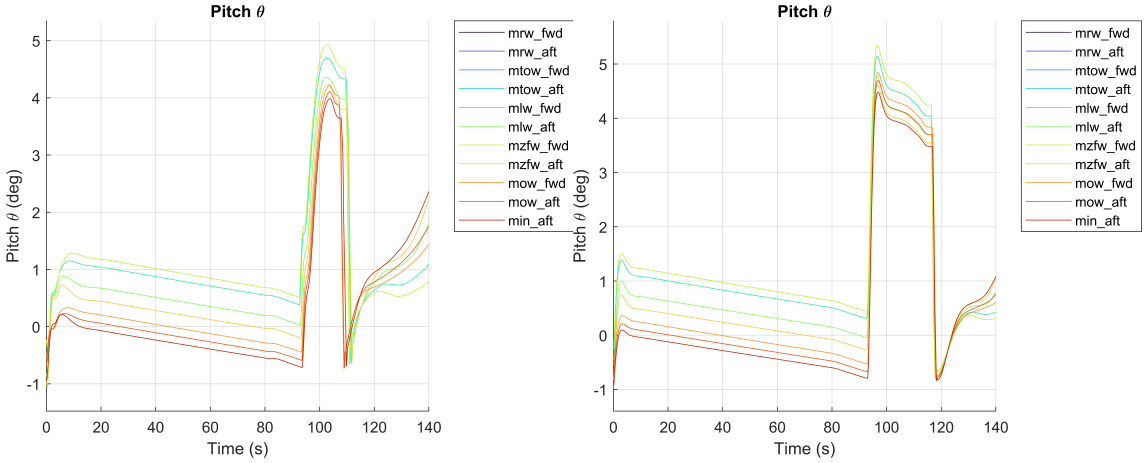

(a) PID **(b)** LQI

Figure 4.18: Pitch angle plot for landing manoeuvre using PID (4.18a) and LQI (4.18b) controllers

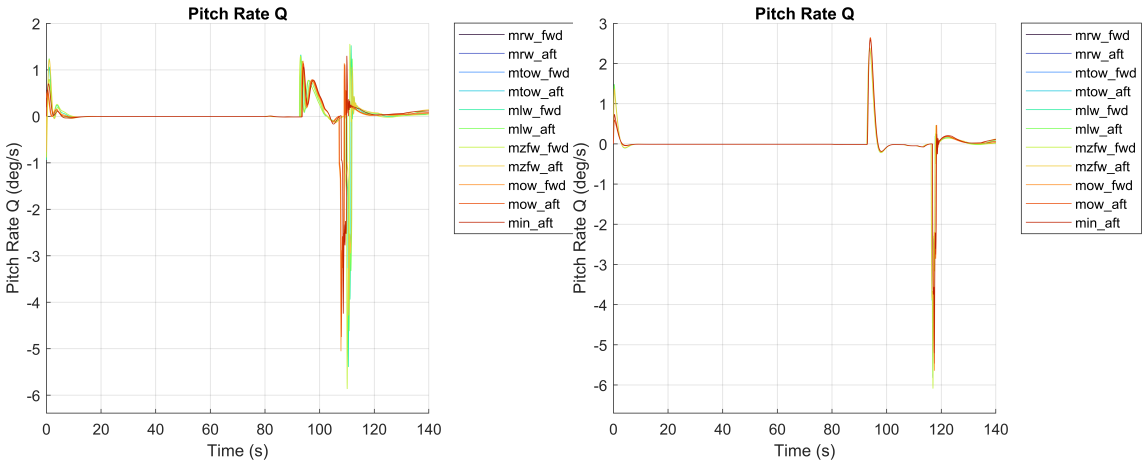

(a) PID **(b)** LQI

Figure 4.19: Pitch rate angle plot for landing manoeuvre using PID (4.19a) and LQI (4.19b) controllers

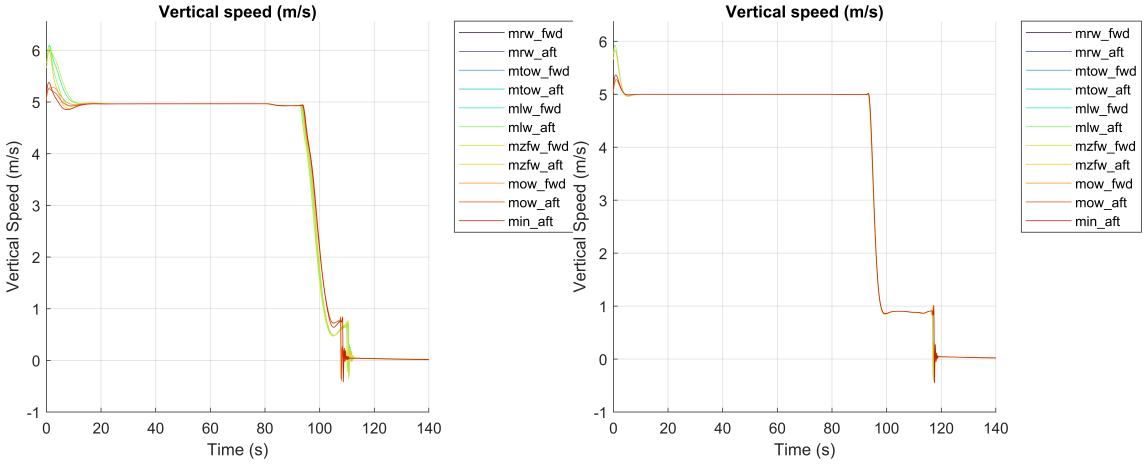

(a) PID **(b)** LQI

Figure 4.20: Vertical speed plot for landing manoeuvre using PID (4.20a) and LQI (4.20b) controllers

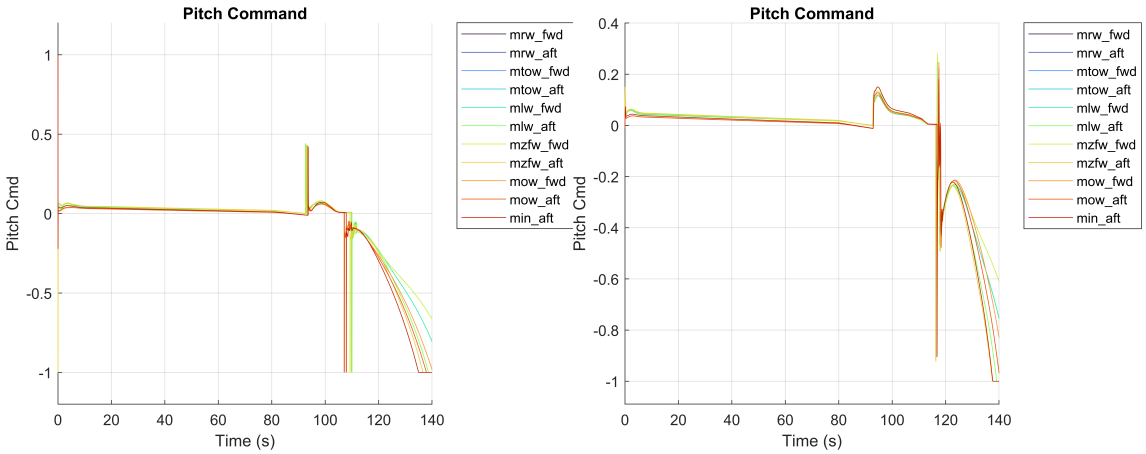

(a) PID **(b)** LQI

Figure 4.21: Pitch command plot for landing manoeuvre using PID (4.21a) and LQI (4.21b) controllers

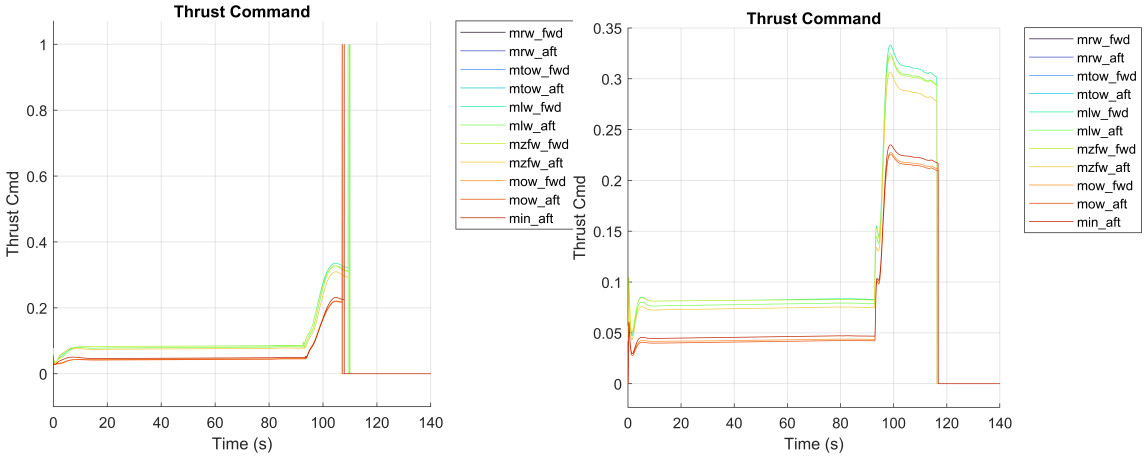

(a) PID **(b)** LQI

Figure 4.22: Thrust command plot for landing manoeuvre using PID (4.22a) and LQI (4.22b) controllers

4.2 Failures

The LQI autopilot was tested for the case where the outer left motor was inoperable. This OEI case is of great interest as many manoeuvres in the CS-25 certification require this condition to be met [3]. It is also interesting as a way to evaluate how the autopilot reacts to the loss of one motor as a large yawing moment is introduced by the imbalance in thrust. The case where the control surfaces had restricted ranges was evaluated however it has been omitted from this section for reasons described in the discussion section below (5).

4.2.1 Roll manoeuvre

Without the thrust from the failed motor the aircraft, in the configuration used in this project, was unable to produce the thrust needed to maintain the required climb rate. This was evident by the thrust command being at its maximum and the altitude trajectory not keeping up with the reference. The result was the aircraft eventually stalling and in some cases going into an unrecoverable dive.

4.2.2 Takeoff

The takeoff with failures was evaluated using the improved takeoff autopilot as it produced the takeoff trajectories most representative of reality. During the OEI acceleration phase the landing gear assists in keeping the aircraft straight. Once the aircraft begins to rotate and lift off the yaw command spikes to keep the aircraft straight. This large yaw command causes the aircraft to roll resulting in a large roll command to combat this. As the airspeed continues to increase the control surfaces gain authority and the amount of control action decreases. The airspeed retains a positive gradient throughout and the pitch rate doesn't show any abnormally large swings. The reduced thrust results in a longer time for all stages of takeoff however

the aircraft is able to successfully take off and climb with one motor failed.

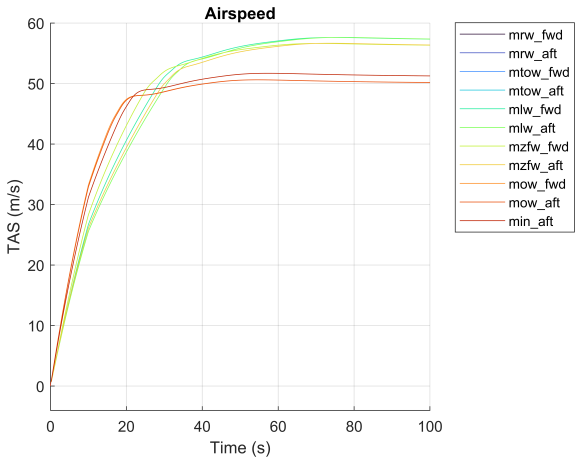

Figure 4.23: Airspeed plot for OEI takeoff manoeuvre using LQI controller

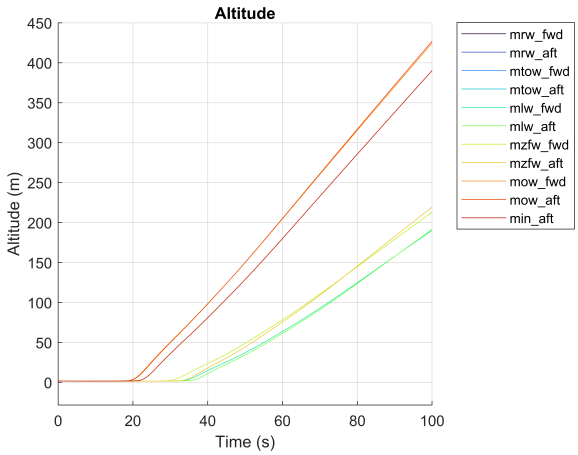

Figure 4.24: Altitude plot for OEI takeoff manoeuvre using LQI controller

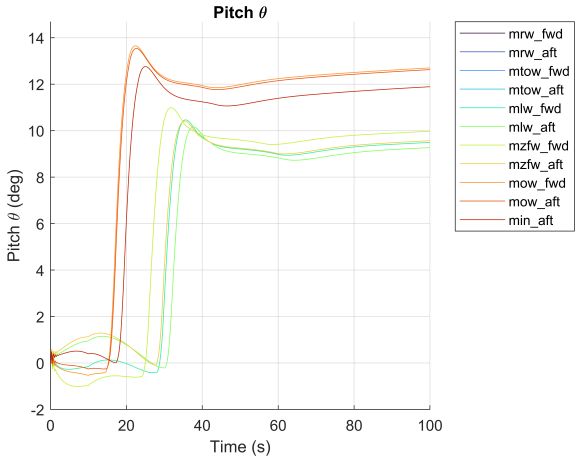

Figure 4.25: Pitch angle plot for OEI takeoff manoeuvre using LQI controller

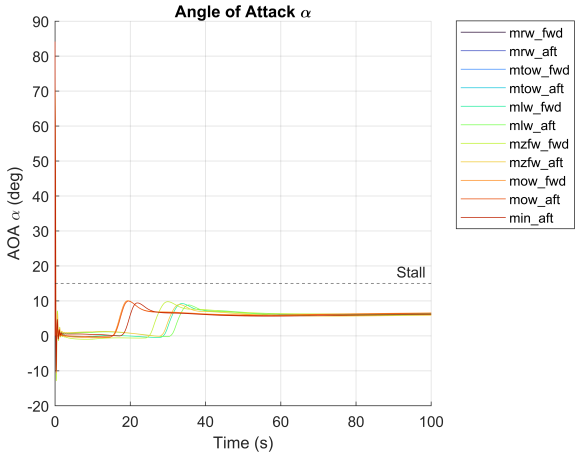

Figure 4.26: Angle of attack plot for OEI takeoff manoeuvre using LQI controller

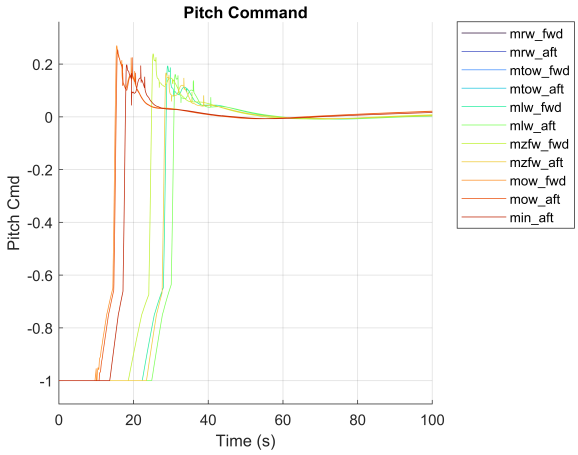

Figure 4.27: Pitch command plot for OEI takeoff manoeuvre using LQI controller

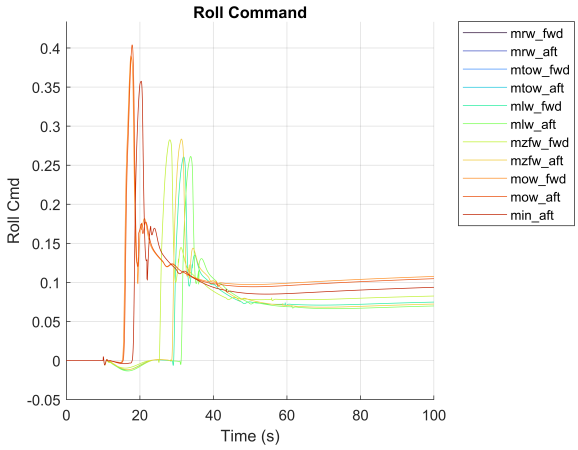

Figure 4.28: Roll command plot for OEI takeoff manoeuvre using LQI controller

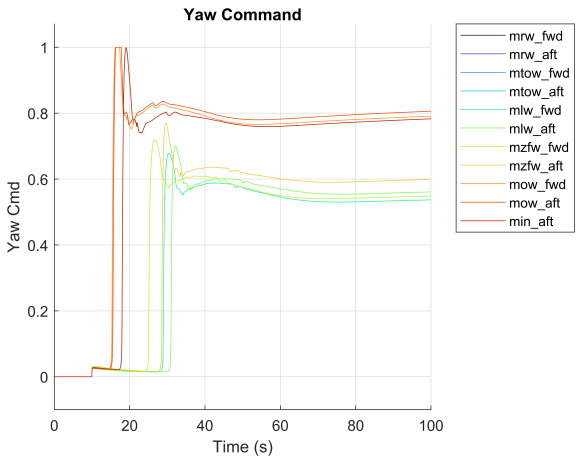

Figure 4.29: Yaw command plot for OEI takeoff manoeuvre using LQI controller

4.2.3 Landing

The OEI landing case did not suffer from the reduced thrust as it never exceeded 50% as shown in figure 4.36. The approach phase shows very similar behaviour compared to the AEO case with the slight roll and yaw command being the primary difference. During the flare when the thrust command increased, and the yaw moment due to the thrust imbalance increased, the raw and roll commands both increase to combat this. The final vertical speed is in a similar range compared to the AEO case and at the desired level.

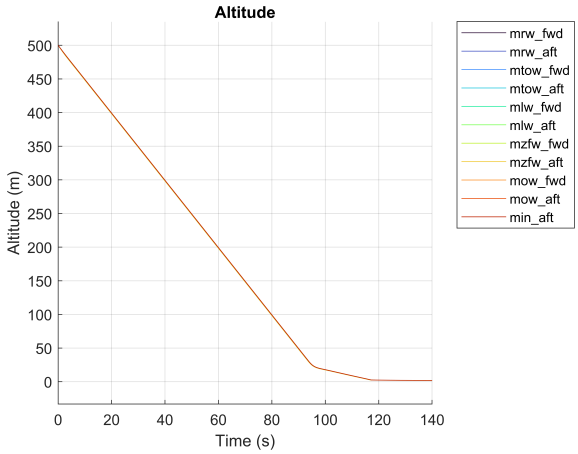

Figure 4.30: Altitude plot for OEI landing manoeuvre using LQI controller

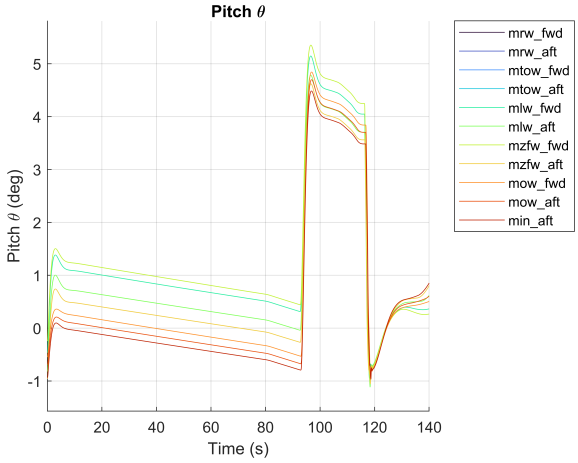

Figure 4.31: Pitch angle plot for OEI landing manoeuvre using LQI controller

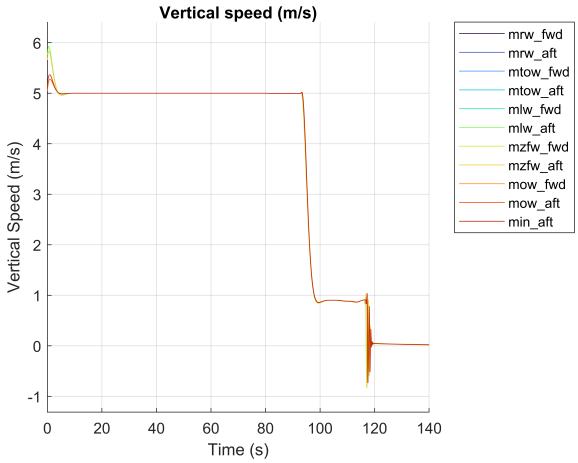

Figure 4.32: Vertical speed plot for OEI landing manoeuvre using LQI controller

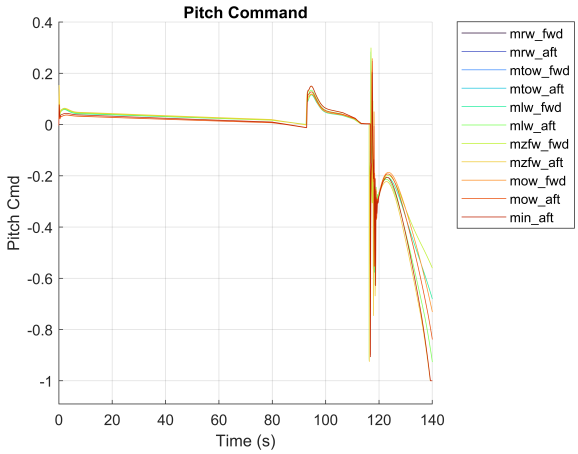

Figure 4.33: Pitch command plot for OEI landing manoeuvre using LQI controller

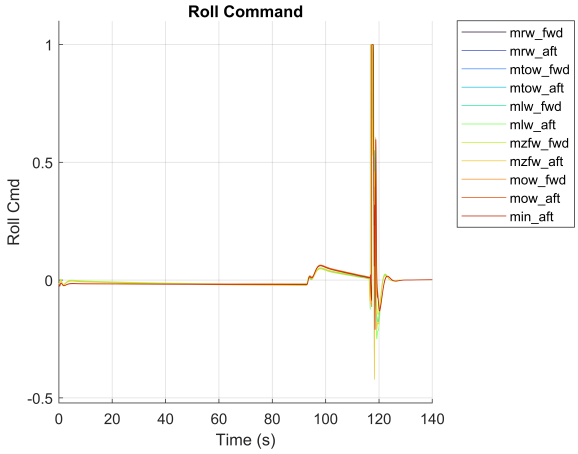

Figure 4.34: Roll command plot for OEI landing manoeuvre using LQI controller

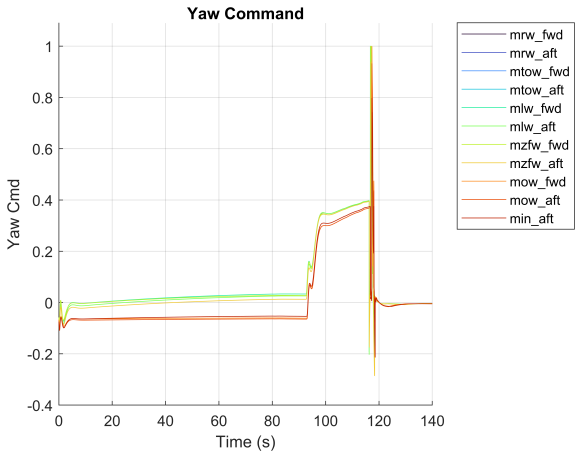

Figure 4.35: Yaw command plot for OEI landing manoeuvre using LQI controller

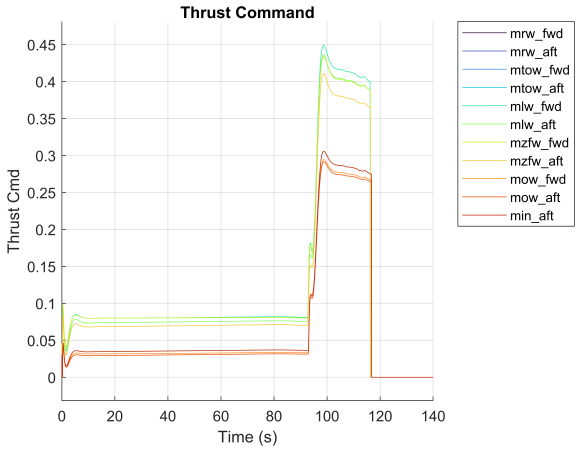

Figure 4.36: Thrust command plot for OEI landing manoeuvre using LQI controller

4.3 Disturbances

To test the robustness of the controller a disturbance was added in the form of wind shear as discussed in section 3.7.2. The wind shear model was chosen as it most closely resembled the type of conditions the tests would be performed in with the real aircraft. The wind speed was set to 30 knots at 10m height which corresponds to the maximum crosswind that is tested for the landing.

4.3.1 Roll manoeuvre

The aircraft was trimmed for the target flight path angle with a 30-knot crosswind acting on the aircraft. During the roll manoeuvre, the aircraft is in a banked turn, this banked turn makes the aircraft change heading. With the change in heading the wind is not pointing in the same direction as the aircraft is trimmed for and therefore showed a tendency to deviate from the desired trajectory towards the end of the manoeuvre. The aircraft reached stall angle during the transition between bank angles as can be seen in figure 4.39.

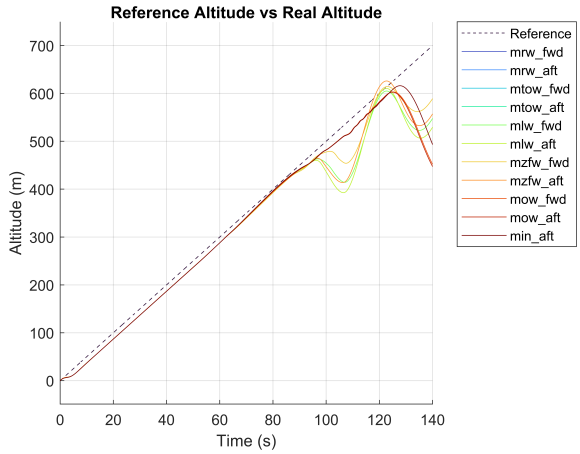

Figure 4.37: Altitude plot for rolling manoeuvre with wind disturbance using LQI controller

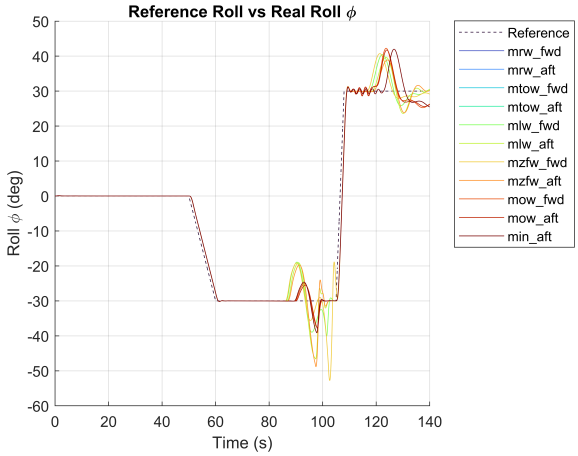

Figure 4.38: Roll plot for rolling manoeuvre with wind disturbance using LQI controller

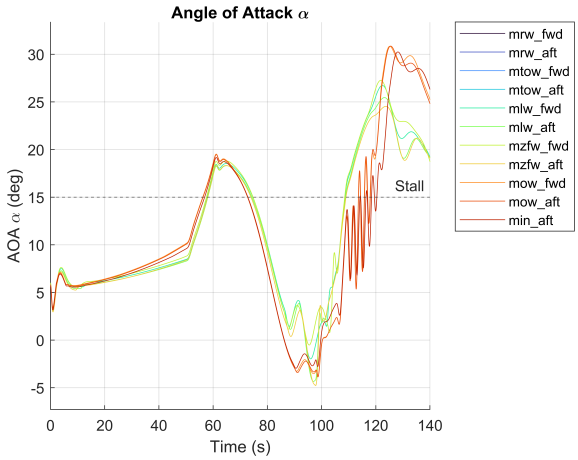

Figure 4.39: Angle of attack plot for rolling manoeuvre with wind disturbance using LQI controller

4.3.2 Takeoff

The aircraft was trimmed for the same 30 knots crosswind as in the roll manoeuvre. The takeoff manoeuvre handled it better than the rolling as can be seen in the very stable climb rate in figure 4.40. This is likely due to the constant heading during the takeoff meaning the aircraft was trimmed for the correct wind direction throughout the manoeuvre. As the aircraft climbed it was able to compensate for the change in wind speeds as it gained altitude. All envelope points were able to keep a steady climb rate throughout takeoff. The starting point of the climb differs between the envelope points due to the VR being different for the different weights and COG placements.

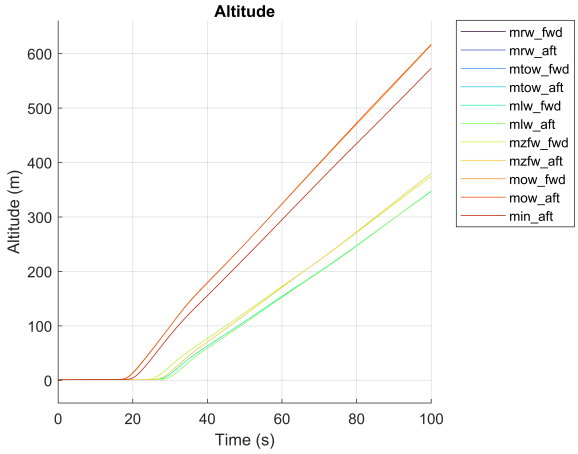

Figure 4.40: Altitude plot for takeoff manoeuvre with wind disturbance using LQI controller

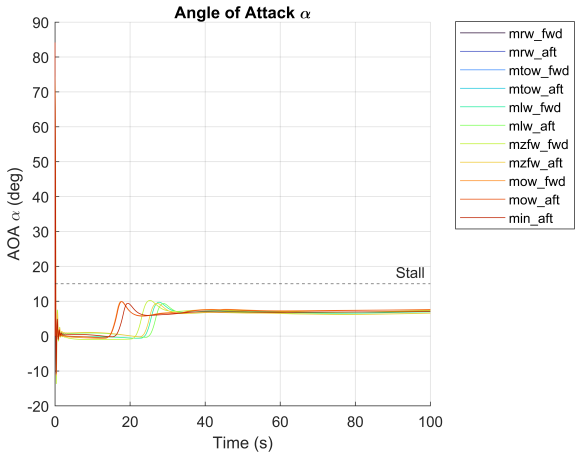

Figure 4.41: Angle of attack plot for takeoff manoeuvre with wind disturbance using LQI controller

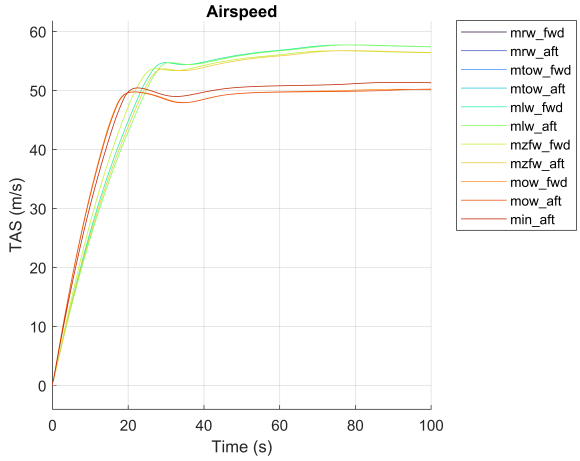

Figure 4.42: Airspeed plot for takeoff manoeuvre with wind disturbance using LQI controller

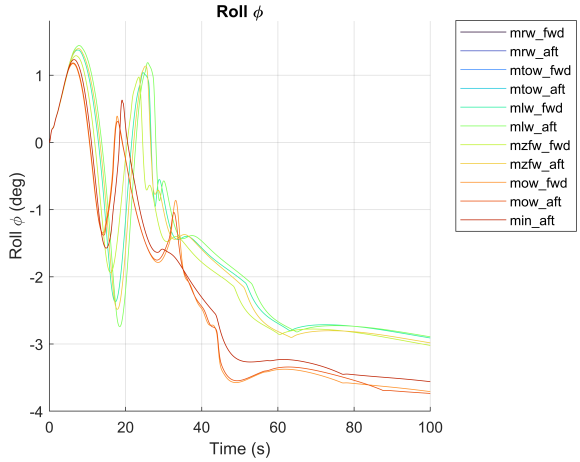

Figure 4.43: Roll angle plot for takeoff manoeuvre with wind disturbance using LQI controller

4.3.3 Landing

The aircraft was able to land for all envelope points with a crosswind of 30 knots. The aircraft was trimmed for the crosswind and the approach flight path angle. The landing with crosswinds was very similar to the ideal case if only viewed in the longitudinal direction. If studying the roll in figure 4.47 and yaw in figure 4.48 it can be seen that the entire approach is done with both a roll and yaw angle. The roll angle reaches a maximum of about 4.5 degrees during the approach but at touchdown, it only has 1 degree of roll angle. The yaw angle at touchdown is relatively large at up to 6 degrees. This results in a lateral velocity causing the aircraft to roll excessively after touchdown.

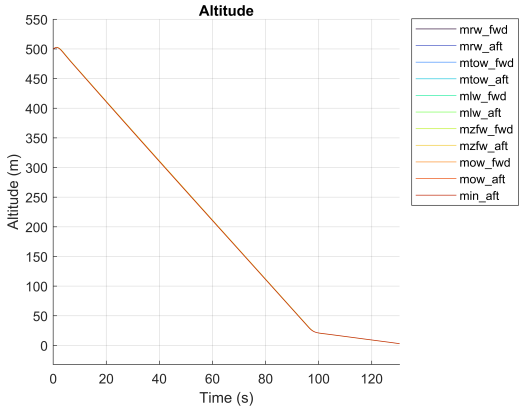

Figure 4.44: Altitude plot for landing manoeuvre with wind disturbance using LQI controller

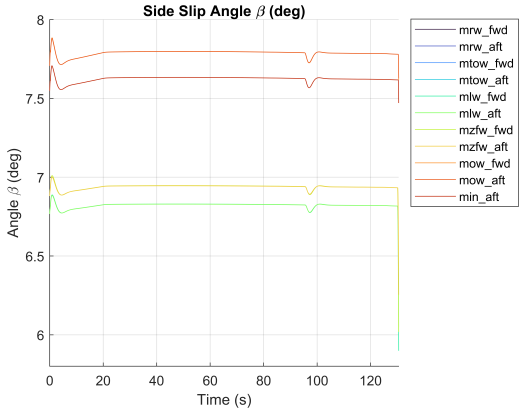

Figure 4.45: Body slip plot for landing manoeuvre with wind disturbance using LQI controller

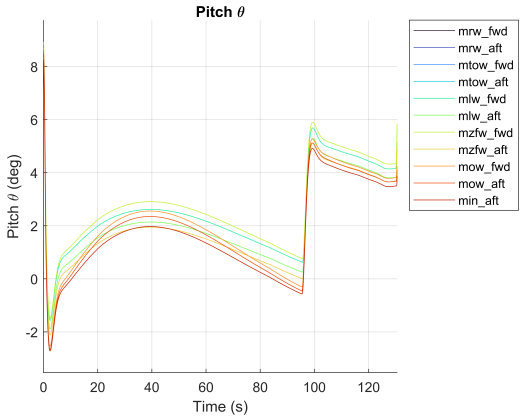

Figure 4.46: Pitch angle plot for landing manoeuvre with wind disturbance using LQI controller

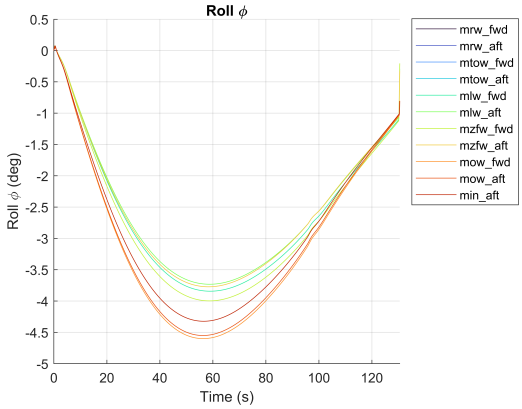

Figure 4.47: Roll angle plot for landing manoeuvre with wind disturbance using LQI controller

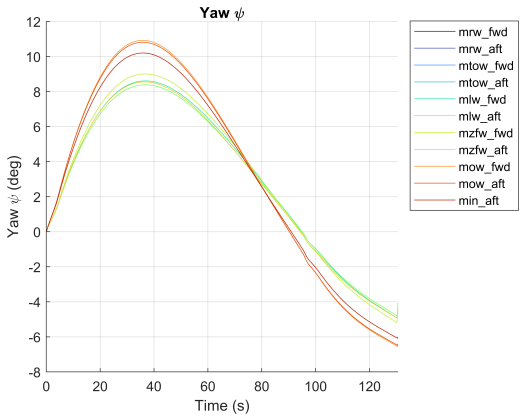

Figure 4.48: Yaw angle plot for landing manoeuvre with wind disturbance using LQI controller

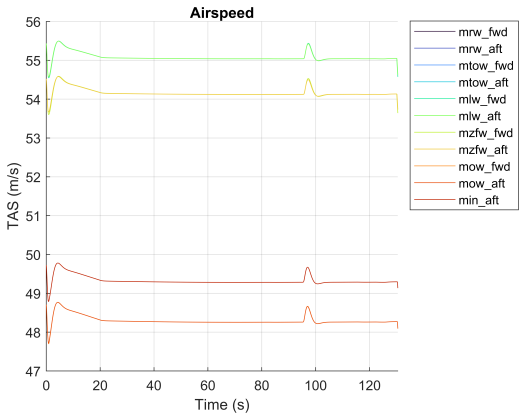

Figure 4.49: Airspeed plot for landing manoeuvre with wind disturbance using LQI controller

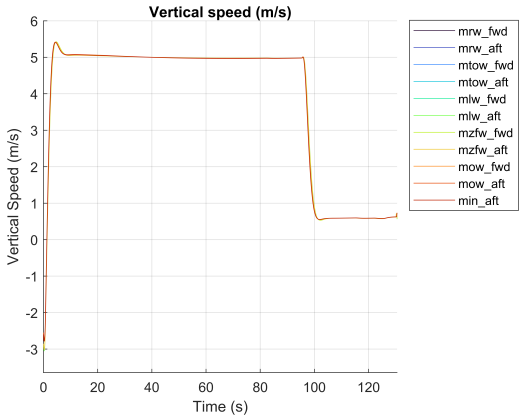

Figure 4.50: Vertical speed plot for landing manoeuvre with wind disturbance using LQI controller

5
Discussion

The aim of the thesis was to develop an autopilot capable of performing a set of manoeuvres that could be used to evaluate an aircraft's performance and gain insight into its flight qualities. This goal was studied using autopilots based on two different controller strategies, PID and LQI. These autopilots were thoroughly tested and evaluated using takeoff, landing and a rolling manoeuvre around the full COG envelope.

5.1 Model

The non-linear model on which the autopilots were tested had been in development for some time and had evolved greatly during that time, with some parts being more complete than others. One part of this model which proved to have some issues in the version used was the ground model. This ground model had some flaws which resulted in the moments and forces spiking very easily. These unpredictable forces and moments could cause the aircraft to become unstable when landing or taking off. Because of this the testing done is constrained to analysis of the aircraft only in the air and the sometimes drastic control action and reaction forces when in contact with the ground are not taken into account. If a higher fidelity and more robust ground model were implemented then manoeuvres such as landing could be analysed further in terms of forces and moments acting on the aircraft.

5.2 Controller evaluation

The PID and LQI autopilots were tested for various manoeuvres and both autopilots were able to complete them with satisfactory results. The results differed between the controllers showing different characteristics in how the reference trajectories were tracked. This was expected as the two approaches are largely different in their formulation with LQI being an optimal controller whereas the PID controller was tuned by hand. Ultimately both the PID and LQI were able to complete the manoeuvres for the ideal case where no disturbance or motor failures were present.

In the roll manoeuvre the PID controller showed a tendency to oscillate in roll towards the end of the transition from one side to the other. This behaviour appeared to be caused by the yaw damper fighting the roll controller at this point. The roll and yaw dynamics are coupled and as such the large amount of rolling that occurs at this point induces some yawing motion. The yaw damper then fights the

motion which results in the observed behaviour. In contrast, the LQI controls both yaw and roll through the lateral controller. This resulted in a smoother level of control without any contradictory control action.

The initial approach to takeoff with both control strategies produced fairly similar results. The PID autopilot showed a faster response with more oscillations in pitch whilst the LQI was slower but smoother. These differences are small enough they could likely be mitigated by alternative tuning of either controller. The overshoot in airspeed produced by both controllers was however undesirable from a flight performance perspective which lead to the development of the improved takeoff. The improved takeoff not only resulted in smoother trajectories without the overshoot in airspeed but was additionally a good example of the ease and flexibility of the LQI approach. To further improve the takeoff there was a change of reference and using the LQI it could be achieved by simply altering the integral state and making some small adjustments on weighting matrices. To accomplish this with the PID approach, there would have had to be a much more involved process of re-tuning and rearranging the inner loop.

The landing manoeuvre produced consistent results between the two controllers and met the target vertical speed values. One flaw with the flare phase was that the autopilot continues to track the target airspeed during the flare. A more correct approach here would be to set the thrust to 0 at the start of the flare and only track vertical speed.

As a whole although both controllers were able to perform the manoeuvres. The LQI approach showed equal or better results than the PID approach in all cases. In addition to this, the fact that the LQI controllers use a plant model as a reference to create the optimal gain matrices, the LQI approach was significantly easier to work with. The developed workflow and the automated process of linearizing, decoupling and creating the LQI gains made the LQI approach the clear preference for continued testing. Because of this the PID was not tested with either the disturbances or failures. The aircraft was able to perform these manoeuvres, as shown by the LQI, but as it would have required more extensive and time-consuming tuning to perform it using the PID, it was decided to not pursue those results.

5.2.1 Failures

Although the failure case of restricted control surfaces was created it was found that the amount of control action required to perform the manoeuvres was heavily influenced by the trimming of the aircraft. Once correctly trimmed the control action was often lower than what the restricted range would affect making the restricted range less interesting. As a result, this particular case was not investigated further and instead the OEI case was given more attention.

For the case with one motor failed the primary effect on longitudinal control was in the reduction in thrust. This loss of thrust resulted in the failure to perform

the rolling manoeuvre as it was not possible to maintain the required climb rate. The takeoff and landing manoeuvres were both performed in a very similar manner when compared to the corresponding AEO cases. The takeoff took slightly longer as the lessened thrust resulted in a slower increase in airspeed and longer time periods between the modes. The landing was able to simply have a higher thrust command with the OEI case requesting up to 45% whilst the AEO case required less than 35%. In the lateral direction, more significant changes were seen. The roll and yaw commands, which were almost entirely inactive during the AEO case, show large values with the takeoff yaw command being the most drastic. Particularly for the lower weight cases, where the takeoff speed is lower and the control surfaces have less authority, the yaw command is close to 80% and even saturates as the aircraft begins to rotate. During landing the effects are lessened as the thrust command is significantly lower however some action is still required to maintain the correct attitude. Despite the failure, the autopilot is still able to successfully complete the takeoff and landing manoeuvres.

5.2.2 Disturbances

When running the manoeuvres with wind disturbance, shown in section 4, the roll manoeuvre struggled the most. This was reflected by the loss of altitude tracking and stalls seen in figures 4.37 and 4.39. This can be attributed to the heading change of the aircraft. The aircraft was trimmed at its starting position before beginning to climb or roll. As the roll manoeuvre was performed it did a banked turn changing the heading angle of the aircraft. As the heading angle changed more and more the wind direction changed from the initial crosswind. This in turn changed the trim condition completely and effectively took the aircraft far from its linearisation point. The final result is instability and a failure to complete the manoeuvre. The autopilot was able to successfully approach the runway but was unable to touch-down and derotate. This was due to the lateral velocity causing the aircraft to roll at touchdown. A possible solution would be to implement tracking on the direction of travel, allowing the aircraft to approach with a crab angle and ensure the direction of travel was parallel with the runway. Then, during the flare, the aircraft would need to quickly straighten out and touch down before starting to drift sideways. Takeoff with wind disturbance was successful for all COG cases with the angle of attack and altitude plots being very similar to the ideal case. The primary difference for the case with disturbance was the oscillations in roll at the start of the manoeuvre which stabilise as the airspeed increases and the control surfaces gain authority.

All final tests were performed with the wind shear model but an attempt was made using both the constant wind and the Dryden turbulence model. There were several reasons behind not using the Dryden turbulence wind model. The first reason is that there was no requirement from the CS-25 that the crosswinds had to be turbulent and the extra turbulence made it significantly harder for the aircraft to land. The second reason was that the LQI was never created to be able to handle any kind of noisy disturbances. The integral term of the LQI is able to handle the slow varying wind of the wind shear by integrating the error in trajectory caused by the wind

model. If the Dryden wind model was to be used it would not be able to react to the higher frequency disturbances as the LQI is not designed to handle this type of uncertainty and disturbance [39].

5.2.3 Autopilot flexibility

The development of all controllers and the tests performed during this thesis was done with one single aerodynamic model which was provided at the beginning of the thesis. This was done to keep the results consistent between versions and controllers. During the thesis however, a new iteration of the aircraft aerodynamics was released and to test the usage of the controller it was moved over to the new model. Running the autopilot with completely new aerodynamics, the LQI autopilot was able to perform all the manoeuvres discussed without any problems or the need for additional tuning. This highlighted the robustness of the model-based approach for an environment where the model is going to go through many frequent iterations.

6
Conclusion and Future work

The autopilot's purpose was to speed up the iterative development process by acting as a test pilot and a tool to quickly gather data about the current version of the aircraft. It was found that a model-based approach suited this application best as it removed the manual process involved in the tuning of the controllers with any model changes. The autopilot was able to consistently perform all required manoeuvres and provide useful data on the current iteration of the aircraft. Using the envelope testing the aircraft designers are able to quickly and efficiently find flaws in either the aircraft model or design that are only visible at certain envelope points. As there are 11 different envelope points on this aircraft, using a test pilot would require more time and produce less repeatable results than the autopilot. Although useful as a tool, the developed autopilot is not able to fully replace a test pilot. A test pilot is better able to give an indication of how the aircraft feels or how easy it is to fly.

The controllers implemented were a PID and a LQI. Due to the PID being a classical controller which is not based on the model it quickly became irrelevant for the industrial purpose of iterative development as it required constant tuning. During the testing and development of the LQI it was noticed that a more robust controller would be necessary to better handle wind disturbances. The model-based approach of the LQI controller worked well for accounting for changes to the model.

The post-processing scripts created, such as the failure detection, are very limited in their current functionality and could greatly benefit from further improvement. Some recommendations would be attempting to quantify the ease of performing the manoeuvre by looking at the rate of change and magnitude of the control action. Further improvements could also be investigated to allow for more robust disturbance handling or to automatically re-trim when deviating too far from the linearization point. The implementation of more manoeuvres could allow the designers to gain more insight into the aircraft's performance in more scenarios. Additionally, a specific focus on improving individual manoeuvres could potentially yield further results and allow for tougher disturbance levels to be handled. Finally extending this study into further types of controllers could produce interesting results and perhaps be better able to handle alternative disturbance types.

Bibliography

[1] Tobias Müller. "Airbus versus boeing – an updated analysis of the duopoly". In: *Journal of Airline and Airport Management* 9.1 (2019), pp. 1–22.

[2] Roberto Merino Martínez. "Design and analysis of the controland stability of a blended wingbody aircraft". MA thesis. Royal Institute of Technology (KTH), 2014.

[3] *Certification specifications and acceptable means of compliance for large aeroplanes (cs-25)*. European Union Aviation Safety Agency.

[4] Justin P Rohrer and John W Robinson. "The role of iteration in the design of spacecraft". In: *Journal of spacecraft and rockets* 41.3 (2004), pp. 429–436.

[5] Michael Grässlin and Björn Nagel. "Analysis of design iterations in aircraft design". In: *10th AIAA Aviation Technology, Integration and Operations Conference (ATIO)*. AIAA. 2010.

[6] Gangadhar B. Kallur. "History of autopilot".

[7] Brian L. Stevens and Frank L. Lewis. *Aircraft control and simulation*. Ed. by John wiley and sons inc. Wiley-interscience, 1939.

[8] Online. Feb. 2023. URL: https://www.garmin.com/en-US/p/70143.

[9] Francisco Gavilan, Rafael Vazquez, and Sergio Esteban. "Trajectory tracking for fixed-wing uav using model predictive control and adaptivebackstepping". In: *IFAC-PapersOnLine 48-9*. 2015.

[10] Julian Theis et al. "Robust autopilot design for landing a large civil aircraft in crosswind". In: *Control Engineering Practice* 76 (2018), pp. 54–64. ISSN: 0967-0661. DOI: https://doi.org/10.1016/j.conengprac.2018.04.010. URL: https://www.sciencedirect.com/science/article/pii/S0967066118300911.

[11] Luke Keating and Dermot Geraghty. "A model predictive control based autopilot for aircraft". In: *2022 13th International Conference on Mechanical and Aerospace Engineering (ICMAE)*. 2022, pp. 347–351. DOI: 10.1109/ICMAE56000.2022.9852882.

[12] Hou In Leong, Shahriar Keshmiri, and Rylan Jager. "Evaluation of a cots autopilot and avionics system for uav's". In: *AIAA Aerospace Conference 2009-1963*. 2009.

[13] Volodymyr Gritsenko et al. "Integral adaptive autopilot for an unmanned aerial vehicle". In: *ISSN: 1648-7788 / eISSN: 1822-41802018 Volume 22 Issue 4: 129–135* (2018).

[14] HaiYang Chao, YongCan Cao, and YangQuan Chen. "Autopilots for small unmanned aerial vehicles: a survey". In: *International Journal of Control, Automation, and Systems 8(1):36-44* (2010).

[15] Mudassir Lone and Alastair Cooke. “Review of pilot models used in aircraft flight dynamics”. In: *Aerospace Science and Technology* 34 (2014), pp. 55–74. ISSN: 1270-9638. DOI: https://doi.org/10.1016/j.ast.2014.02.003. URL: https://www.sciencedirect.com/science/article/pii/S1270963814000285.

[16] Adnan Causevic, Daniel Sundmark, and Sasikumar Punnekkat. “Factors limiting industrial adoption of test driven development: a systematic review”. In: *2011 Fourth IEEE International Conference on Software Testing, Verification and Validation*. 2011, pp. 337–346. DOI: 10.1109/ICST.2011.19.

[17] MJ Abzug and EE Larrabee. “Automatic flight control systems”. In: *Airplane Aerodynamics and Performance*. John Wiley & Sons, Inc., 2005, pp. 14–1.

[18] G. E. Cooper and R. P. Harper. “The use of pilot rating in the evaluation of aircraft handling qualities”. In: *AGARD Conference Proceedings*. Vol. 66. 1969, pp. 1–12.

[19] European Union Aviation Safety Agency. *Electric and hybrid-electric propulsion for aviation - EASA perspective*. Tech. rep. European Union Aviation Safety Agency, 2019.

[20] Javiera Muñoz-Mendoza and Felipe Arenas-Arroyo. “Lithium mining in Chile: Exploring the relationship between ecosystem and human well-being”. In: *Ecosystem Services* 29 (2018), pp. 445–455. DOI: 10.1016/j.ecoser.2017.12.019.

[21] Gayathri Vaidyanathan. “The global e-waste burden”. In: *Nature* 553.7689 (2018), pp. 20–22.

[22] Thomas R. Yechout et al. *Introduction to aircraft flight mechanics*. Ed. by Joseph A. Schetz. American institure of aeronautics and astronautics inc, 2003.

[23] *Angle of attack (aoa)*. https://www.skybrary.aero/articles/angle-attack-aoa. Accessed 2023-03-09.

[24] Sebastian Ruder. *An overview of gradient descent optimization algorithms*. 2017. arXiv: 1609.04747 [cs.LG].

[25] MathWorks. *MathWorks: linearizeOptions*. https://www.mathworks.com/help/slcontrol/ug/linearizeoptions.html. Accessed: 2020-05-05.

[26] Michael V. Cook. *Flight dynamics principles*. Third. Elsevier Ltd, 2013.

[27] Juan J. Gude, E. Kahoraho, and Josu Etxaniz. “Practical aspects of pid controllers: An industrial experience”. In: Sept. 2006, pp. 870–878. DOI: 10.1109/ETFA.2006.355215.

[28] Gene F Franklin, J David Powell, and Michael L Workman. *Feedback control of dynamic systems*. 3rd ed. Addison-Wesley, 1994.

[29] Alexandre C. Dimian, Costin S. Bildea, and Anton A. Kiss. “Chapter 15 - Plantwide Control”. In: *Integrated Design and Simulation of Chemical Processes*. Ed. by Alexandre C. Dimian, Costin S. Bildea, and Anton A. Kiss. Vol. 35. Computer Aided Chemical Engineering. Elsevier, 2014, pp. 599–647. DOI: https://doi.org/10.1016/B978-0-444-62700-1.00015-2. URL: https://www.sciencedirect.com/science/article/pii/B9780444627001000152.

[30] E.H.J. Pallett. *Automatic Flight Control Systems*. en. Third. Butterworth-Heinemann, 2007.

[31] George Ellis. “Chapter 6 - Four Types of Controllers”. In: *Control System Design Guide (Fourth Edition)*. Ed. by George Ellis. Fourth Edition. Boston: Butterworth-Heinemann, 2012, pp. 97–119. ISBN: 978-0-12-385920-4. DOI: https://doi.org/10.1016/B978-0-12-385920-4.00006-0. URL: https://www.sciencedirect.com/science/article/pii/B9780123859204000060.

[32] Magnus Vestergren. “Automatic takeoff and landing of unmanned fixed wing aircrafts”. MA thesis. Linköping University, 2016.

[33] Henric Jorholm Andersson and Carl Folkesson. “Lateral-directional controller design for an electric aircraft”. MA thesis. Chalmers University of Technology, 2022.

[34] Min Liu et al. “Application of LQI control in permanent magnet synchronous motor based on parameter identification”. In: *Journal of Physics: Conference Series* 1105.1 (2018), p. 012050.

[35] Jenny Aurora Frøland Steindal. “Gain scheduled controller with bumpless transfer for an unmanned surface vehicle”. MA thesis. Norwegian University ofScience and Technology, 2019.

[36] *Weight and balance*. June 2016. URL: https://code7700.com/weight_and_balance.htm#ref.

[37] U.S. Military Specification. *MIL-F-8785C*. Nov. 1980.

[38] Pramod Abichandani et al. “A Survey of Wind Measurement and Simulation Techniques in Multi-Rotor Small Unmanned Aerial Vehicles”. In: *IEEE Access* PP (Mar. 2020), pp. 1–1. DOI: 10.1109/ACCESS.2020.2977693.

[39] Bingzhao Gao et al. “Linear quadratic output regulator with disturbance rejection: application to vehicle launch control”. In: *American Control Conference*. Sheraton, Seattle Hotel, May 2017.

A

Appendix 1

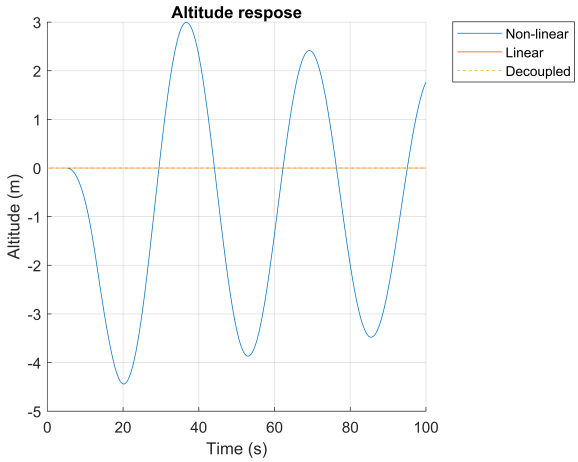

Figure A.1: Altitude response to a 0.5s square pulse with an amplitude of 0.1 applied to roll command

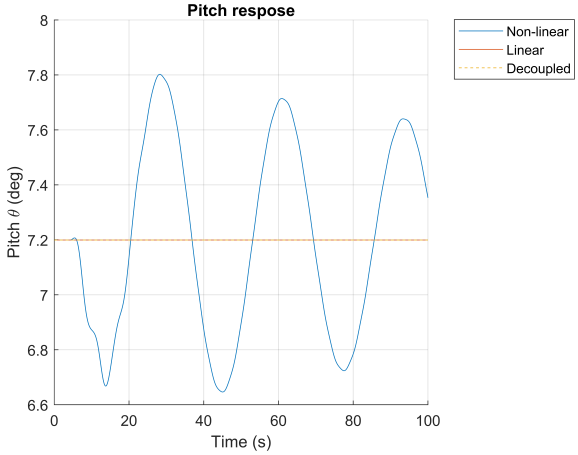

Figure A.2: Pitch response to a 0.5s square pulse with an amplitude of 0.1 applied to roll command

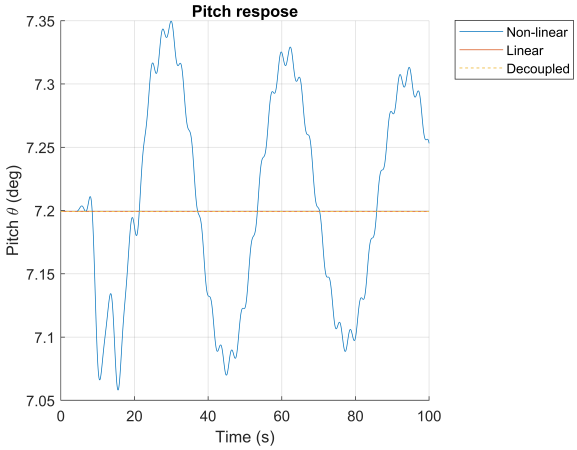

Figure A.3: Roll response to a 0.5s square pulse with an amplitude of 0.1 applied to pitch command

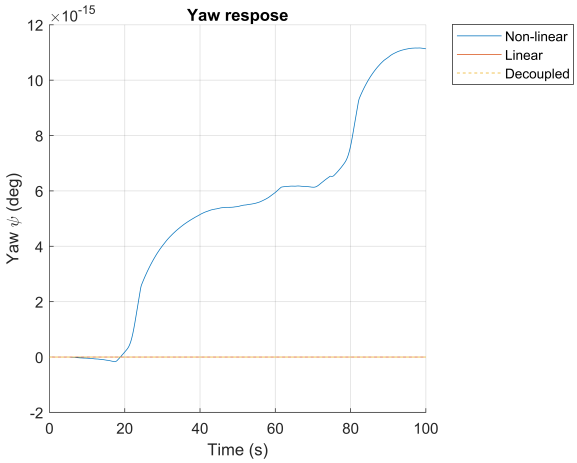

Figure A.4: Yaw response to a 0.5s square pulse with an amplitude of 0.1 applied to pitch command

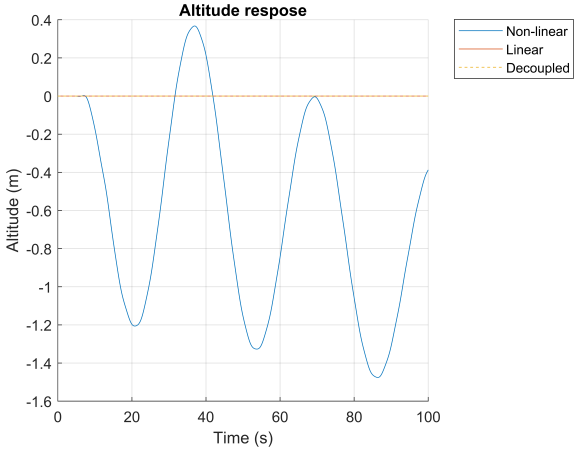

Figure A.5: Altitude response to a 0.5s square pulse with an amplitude of 0.1 applied to yaw command

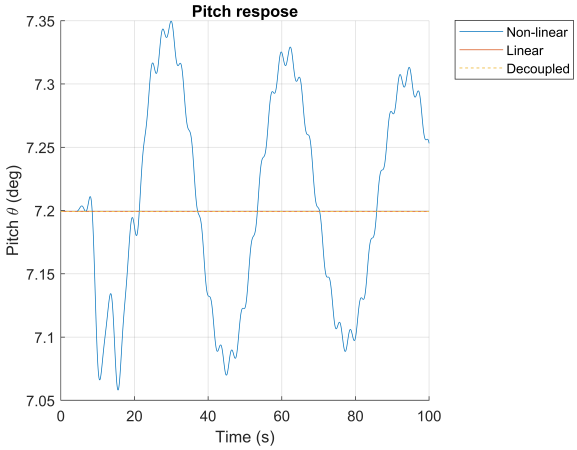

Figure A.6: Pitch response to a 0.5s square pulse with an amplitude of 0.1 applied to yaw command

B

Appendix 2

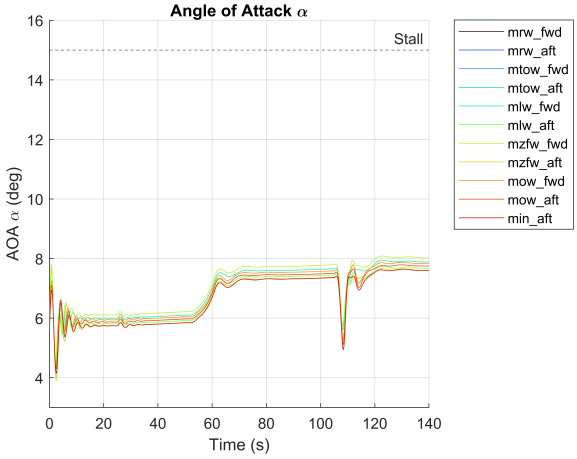

(a) PID

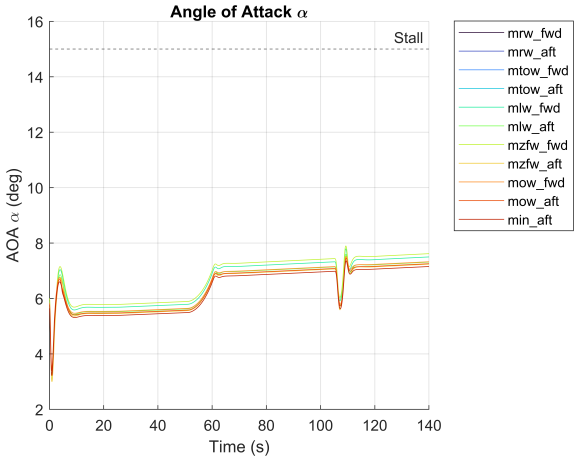

(b) LQI

Figure B.1: Angle of attack plot for rolling manoeuvre while climbing using PID (B.1a) and LQI (B.1b) controllers

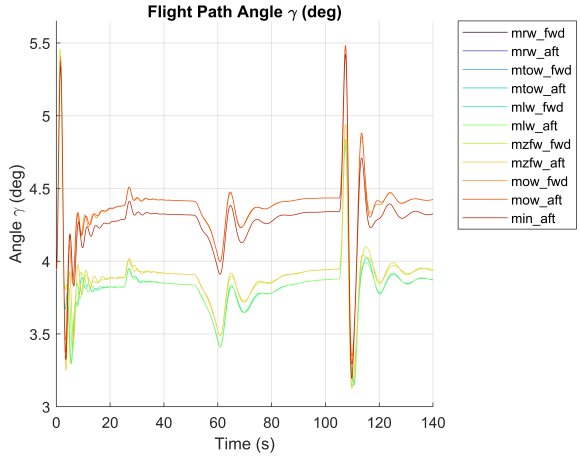

(a) PID

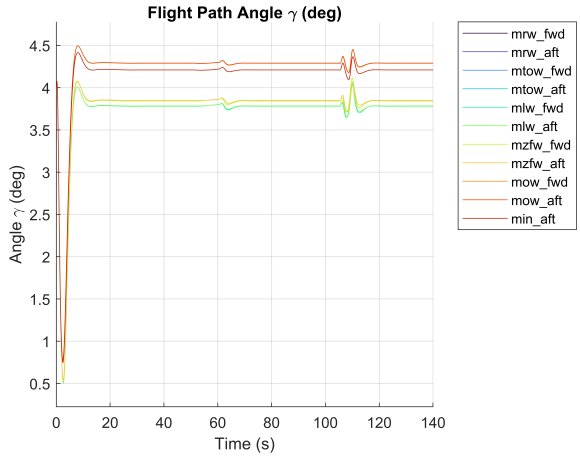

(b) LQI

Figure B.2: Flight path angle plot for rolling manoeuvre while climbing using PID (B.2a) and LQI (B.2b) controllers

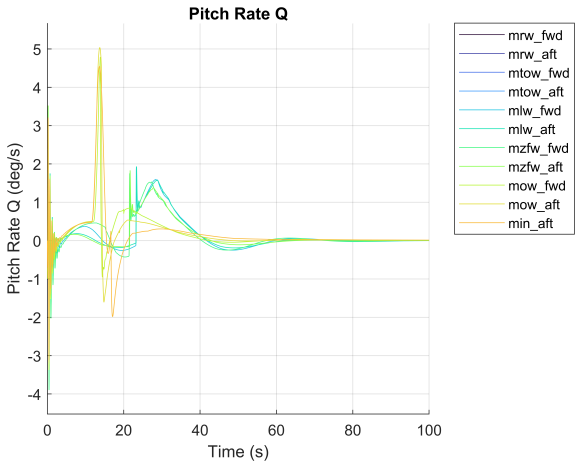

Figure B.3: Pitch rate plot for takeoff manoeuvre LQI controller

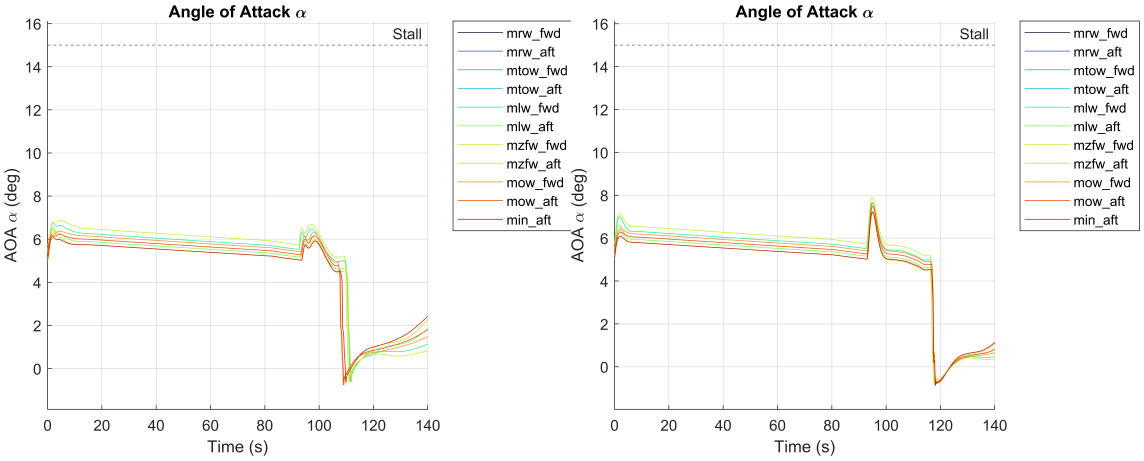

(a) PID **(b)** LQI

Figure B.4: Angle of Attack plot for landing manoeuvre using PID (B.4a) and LQI (B.4b) controllers

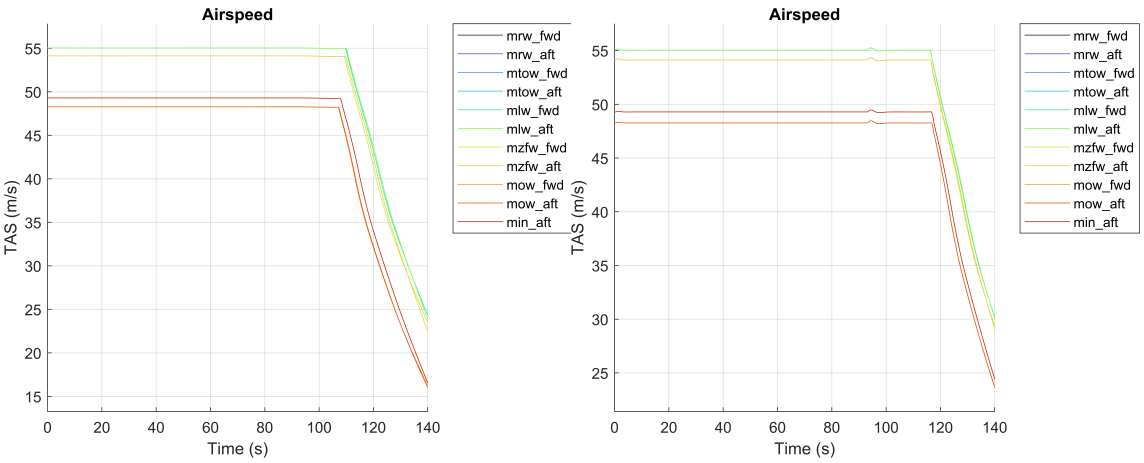

(a) PID **(b)** LQI

Figure B.5: Airspeed plot for landing manoeuvre using PID (B.5a) and LQI (B.5b) controllers

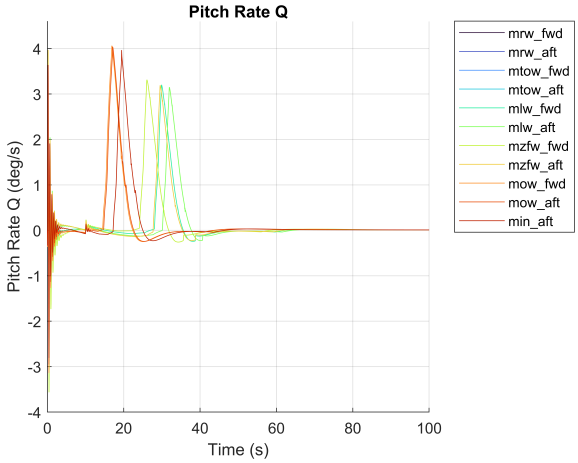

Figure B.6: Pitch rate plot for OEI takeoff manoeuvre using LQI controller

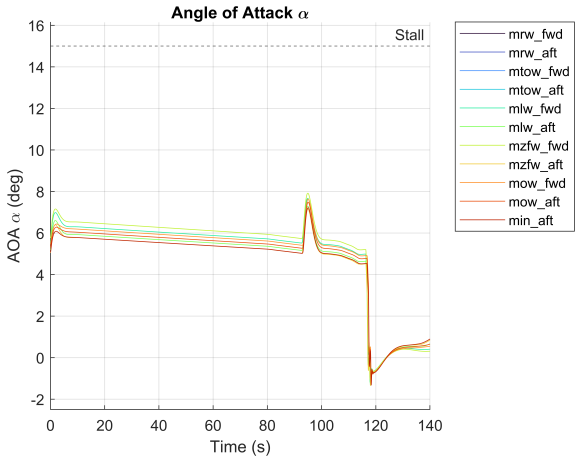

Figure B.7: Angle of attack plot for OEI landing manoeuvre using LQI controller

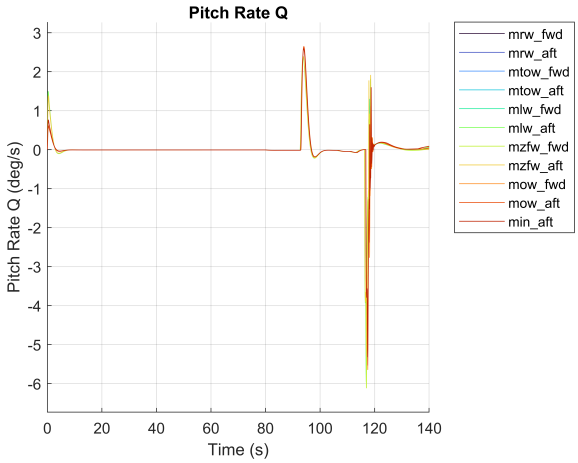

Figure B.8: Pitch rate plot for OEI landing manoeuvre using LQI controller

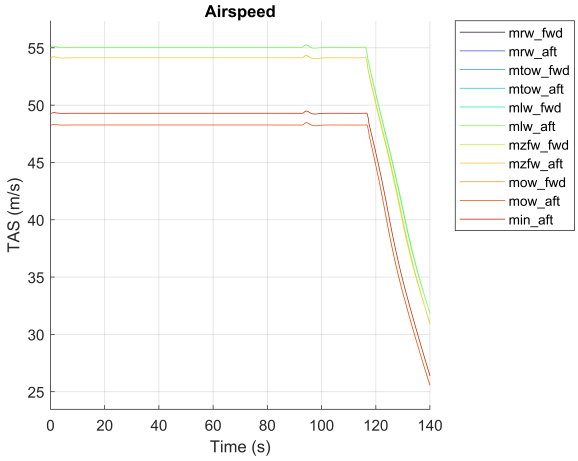

Figure B.9: Airspeed plot for OEI landing manoeuvre using LQI controller

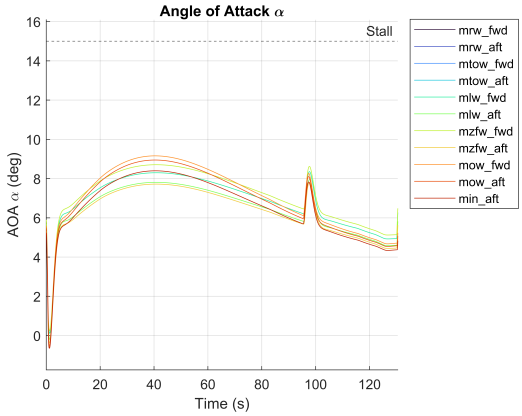

Figure B.10: Angle of attack plot for landing manoeuvre with wind disturbance using LQI controller

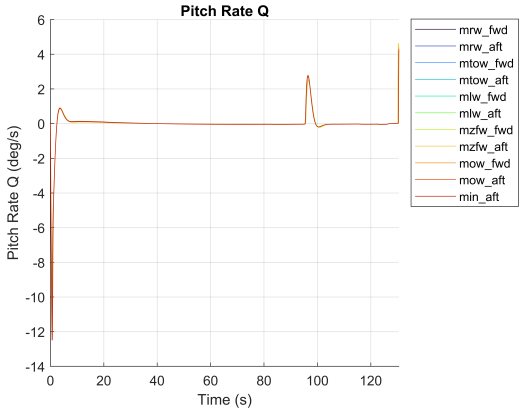

Figure B.11: Pitch rate plot for landing manoeuvre with wind disturbance using LQI controller

DEPARTMENT OF SOME SUBJECT OR TECHNOLOGY
CHALMERS UNIVERSITY OF TECHNOLOGY
Gothenburg, Sweden
www.chalmers.se

CHALMERS
UNIVERSITY OF TECHNOLOGY